



HAL
open science

Harnessing the Vnn1 pantetheinase pathway boosts short chain fatty acids production and mucosal protection in colitis

Virginie Millet, Thomas Gensollen, Michael Maltese, Melanie Serrero, Nathalie Lesavre, Christophe Bourges, Christophe Pitaval, Sophie Cadra, Lionel Chasson, Thien Phong Vu Man, et al.

► To cite this version:

Virginie Millet, Thomas Gensollen, Michael Maltese, Melanie Serrero, Nathalie Lesavre, et al.. Harnessing the Vnn1 pantetheinase pathway boosts short chain fatty acids production and mucosal protection in colitis. *BMJ - British Medical Journal*, 2022, 10.1136/gutjnl-2021-325792 . hal-03975895

HAL Id: hal-03975895

<https://amu.hal.science/hal-03975895>

Submitted on 6 Feb 2023

HAL is a multi-disciplinary open access archive for the deposit and dissemination of scientific research documents, whether they are published or not. The documents may come from teaching and research institutions in France or abroad, or from public or private research centers.

L'archive ouverte pluridisciplinaire **HAL**, est destinée au dépôt et à la diffusion de documents scientifiques de niveau recherche, publiés ou non, émanant des établissements d'enseignement et de recherche français ou étrangers, des laboratoires publics ou privés.

Harnessing the Vnn1 pantetheinase pathway boosts short chain fatty acids production and mucosal protection in colitis

Virginie Millet,¹ Thomas Gensollen,² Michael Maltese,¹ Melanie Serrero,³ Nathalie Lesavre,⁴ Christophe Bourges,⁵ Christophe Pitaval,¹ Sophie Cadra,¹ Lionel Chasson,¹ Thien Phong Vu Man,¹ Marion Masse,¹ Juan Jose Martinez-Garcia,⁶ Fabrice Tranchida,⁷ Laetitia Shintu,⁷ Konrad Mostert,⁸ Erick Strauss,⁸ Patricia Lepage ,⁹ Mathias Chamailard,⁶ Achille Broggi,¹ Laurent Peyrin-Biroulet ,¹⁰ Jean-Charles Grimaud,³ Philippe Naquet,¹ Franck Galland ¹

ABSTRACT

Objective In the management of patients with IBD, there is a need to identify prognostic markers and druggable biological pathways to improve mucosal repair and probe the efficacy of tumour necrosis factor alpha biologics. Vnn1 is a pantetheinase that degrades pantetheine to pantothenate (vitamin B₅, a precursor of coenzyme A (CoA) biosynthesis) and cysteamine. Vnn1 is overexpressed by inflamed colonocytes. We investigated its contribution to the tolerance of the intestinal mucosa to colitis-induced injury.

Design We performed an RNA sequencing study on colon biopsy samples from patients with IBD stratified according to clinical severity and modalities of treatment. We generated the VIVA mouse transgenic model, which specifically overexpresses Vnn1 on intestinal epithelial cells and explored its susceptibility to colitis. We developed a pharmacological mimicry of Vnn1 overexpression by administration of Vnn1 derivatives.

Results VNN1 overexpression on colonocytes correlates with IBD severity. VIVA mice are resistant to experimentally induced colitis. The pantetheinase activity of Vnn1 is cytoprotective in colon: it enhances CoA regeneration and metabolic adaptation of colonocytes; it favours microbiota-dependent production of short chain fatty acids and mostly butyrate, shown to regulate mucosal energetics and to be reduced in patients with IBD. This prohealing phenotype is recapitulated by treating control mice with the substrate (pantetheine) or the products of pantetheinase activity prior to induction of colitis. In severe IBD, the protection conferred by the high induction of VNN1 might be compromised because its enzymatic activity may be limited by lack of available substrates. In addition, we identify the elevation of indoxyl sulfate in urine as a biomarker of Vnn1 overexpression, also detected in patients with IBD.

Conclusion The induction of Vnn1/VNN1 during colitis in mouse and human is a compensatory mechanism to reinforce the mucosal barrier. Therefore, enhancement of vitamin B₅-driven metabolism should improve mucosal healing and might increase the efficacy of anti-inflammatory therapy.

WHAT IS ALREADY KNOWN ON THIS SUBJECT?

- ⇒ Anti-inflammatory antitumour necrosis factor alpha (anti-TNF α) biologics represent the principal treatment of IBD but biomarkers of resistance are still lacking.
- ⇒ Healing of the intestinal barrier becomes a new target in the management of IBD.
- ⇒ Epithelial cell fitness and specific functions such as secretion of mucus or antimicrobial peptides ensure the integrity of the mucosal barrier.
- ⇒ Metabolic alterations in colonocytes are a hallmark of IBD and might depend on defective production of short chain fatty acids by the gut microbiota.

WHAT ARE THE NEW FINDINGS?

- ⇒ The level of colonic VNN1 expression is a marker of IBD severity.
- ⇒ Overexpression of Vnn1 on colonocytes protects from experimental murine colitis.
- ⇒ It reinforces mucosal barrier by preserving colonocyte metabolic activity and favouring beneficial bacterial communities to produce butyrate.
- ⇒ Pharmacological administration of Vnn1 pantetheinase derivatives recapitulates this protection in control C57BL/6 mice, suggesting the possibility of reconditioning gut homeostasis.
- ⇒ Elevation of urinary indoxyl sulfate (IS) follows Vnn1 overexpression.

INTRODUCTION

IBD mostly encompass two disabling, lifelong and incurable disorders, Crohn's disease (CD) and UC,¹ the incidence of which is constantly increasing in high-income countries.² Antitumour necrosis factor alpha (anti-TNF α) biologics, the primary treatment of IBD,^{3,4} fail in 30% patients due to a non-responsiveness or the progressive development of a resistance to therapy, motivating the search for new

HOW MIGHT IT IMPACT ON CLINICAL PRACTICE IN THE FORESEEABLE FUTURE?

- ⇒ A vitamin B₅-dependent pathway is essential for mucosal healing.
- ⇒ Adequate levels of vitamin B₅ should be maintained during the course and treatment of IBD (ie, anti-TNF α) by administering Vnn1 derivatives.
- ⇒ Elevation of urinary IS levels could be a new biomarker of IBD progression and/or therapeutic efficacy.

strategies.^{5,6} The persistence of a mucosal inflammation correlates with the relapses and complications of IBD, which could be due to an incomplete histological remission and healing.^{7,8} Mucosal healing can be regarded as restitution of the intestinal lining and barrier function. Histoendoscopic mucosal healing was defined as attaining both endoscopic and histological improvement (low neutrophil infiltration, absence of crypt destruction and absence of erosion or ulceration), a situation associated with increased rates of long-term clinical remission in IBD.^{9,10} Disruption of the intestinal barrier and repeated epithelial damage have become new targets in the management of these diseases.^{11,12}

An intact mucosal barrier requires the adequate control of epithelial cell fitness, cell-junctions and luminal secretion of mucus or antimicrobial peptides (AMPs).¹³ Transcriptomic and proteomic analyses of gut mucosa in IBD revealed metabolic alterations in colonocytes, including a shift from oxidative phosphorylation (OXPHOS) to glycolysis and a deficit in lipid-dependent energy production,^{14,15} likely as a consequence of reduced production of short chain fatty acids (SCFA) by the gut microbiota.¹⁶ Indeed, butyrate is required for the regulation of stem cell renewal and represents the major energetic substrate through the coenzyme A (CoA)-dependent process of fatty acid β -oxidation (FAO) in mature colonocytes.¹⁷ Therefore, colonocytes might be particularly sensitive to variations in CoA levels.

In eukaryotes, CoA cannot diffuse across membranes and must be synthesised in each cell from cysteine, ATP and pantothenate (Pan) (vitamin B₅).¹⁸ Pan derives either from the degradation of the (acyl-)CoA present in food or the gut microbiome prior to uptake by intestinal cells, or from the systemic recycling of cell-derived CoA.¹⁸ Its availability depends on extracellular CoA degradation by Vnn pantetheinases that hydrolyse CoA-derived pantetheine (PanSH) into cysteamine (CEA) and Pan.^{18–20} The Vnn1 isoform regulates metabolic, inflammatory and cytoprotective programmes in mouse tissues.^{21–25} Highly expressed in ileum, Vnn1 is present at low levels in colonocytes where its expression is inducible by stress.^{26–28} Likewise, the colonic epithelium of patients with IBD displays high VNN1 levels and single nucleotide polymorphisms in the regulatory regions of the gene are associated with high VNN1 expression and disease risk/severity.²⁷ In this report, we monitored VNN1 expression in patients with IBD stratified according to evolution under various therapies and show that the level of VNN1 expression parallels disease severity. We generated VIVA transgenic mice that overexpress Vnn1 specifically in the gut epithelium as is the case in patients. Vnn1 overexpression preserves colonocyte fitness and reinforces the intestinal barrier during colitis. This phenotype is associated with an enrichment in SCFA-producing bacteria, higher faecal butyrate amounts, increased CoA levels and metabolic rewiring in colon. Importantly, the pharmacological administration of Vnn1 pantetheinase derivatives recapitulates this protection in control C57BL/6 mice suggesting the possibility of reconditioning gut homeostasis. Therefore, VNN1

sustains a vitamin B₅-dependent pathway essential for mucosal energetics and healing.

METHODS

Data access

All raw and processed sequencing data generated in this study are accessible on the NCBI Gene Expression Omnibus (GEO) under the meta-series GSE174159 (<https://www.ncbi.nlm.nih.gov/geo/query/acc.cgi?acc=GSE174159>) for human IBD data, and GSE174166 (<https://www.ncbi.nlm.nih.gov/geo/query/acc.cgi?acc=GSE174166>) for mouse dextran sodium sulfate (DSS)-colitis data.

Animal care and treatment

Mice were kept in a specific pathogen-free mouse facility at CIML. Experiments were carried out on female VIVA mice aged 8–17 weeks or wild-type (WT) C57BL/6 controls bred at CIML or purchased from Janvier (France); Vnn1-deficient mice²⁰ and NLRP6-deficient mice.²⁹ For drug treatments, mice were intraperitoneally injected every 2 days for 2 weeks with cysteamine hydrochloride (120 mg/kg) and Pan (500 mg/kg) or D-pantethine (1 g/kg). All reagents were purchased from Sigma-Aldrich. Oral administration of D-pantethine was done by gavage every 2 days at a dose of 150 mg/kg. For microbiota depletion, mice received by gavage a daily dose of 200 μ L of a broad-spectrum antibiotic cocktail consisting of metronidazole (1 mg/mL), vancomycin (0.5 mg/mL), gentamycin (1 mg/mL), neomycin (1 mg/mL) and ampicillin (1 mg/mL) for 10 days.

Experimental colitis induction and scoring

Acute DSS-colitis was induced by a 7-day oral administration of 2% DSS (MP Biomedical) in the drinking water. In the chronic colitis model, mice were treated with 0.75% DSS during 2 weeks, then water for 15 days followed by a second exposition to 0.75% DSS for 2 weeks. Colons were removed, measured, longitudinally cut and coiled with the mucosal layer outwards, then fixed with formol and embedded in paraffin. Swiss rolls were sectioned at 3.5 μ m and stained with H&E. Histological scores were assessed blindly by a pathologist following the criteria described in online supplemental table S1.

Acute TNBS-colitis was induced by intrarectal administration of 2.5% 2,4,6-trinitrobenzene sulfonic acid (TNBS, Sigma-Aldrich) in 50% ethanol. Colons were examined to evaluate the macroscopic lesions according to the Wallace criteria. The disease activity index, ranging from 0 (unaffected) to 12 (severe colitis), was calculated as the total scores of the sum of weight loss, diarrhoea and bleeding.

Histological studies

Vnn1 and Ep-CAM expression was analysed on cryosections using purified 407 (Santa Cruz) and Ep-CAM antibodies (Epitomics), using the secondary Cy3 AffiniPure Donkey Anti-Rat and Alexa Fluor 488 Donkey Anti-Rabbit IgG (H+L), respectively. Slides were mounted in ProLong Gold with 4',6-Diamidino-2-Phenylindole (DAPI) (Invitrogen) and observed with a Zeiss LSM 510 confocal microscope (Carl Zeiss, Jena, Germany).

To monitor cell proliferation and neutrophil infiltration, paraffin sections were stained with the anti-Ki67 antibody (BD Bioscience) and anti-Ly6G antibody (BD Pharmingen), respectively, revealed by the ImmPRESS HRP Goat Anti-Rat IgG Polymer Detection Kit using peroxidase and 3,3'-Diaminobenzidine (DAB) (Vector Laboratories). Five pictures were taken per

swiss-roll and Ki67+ and Ly6G+ cells counted using the ImageJ software and cell count plugin. A standard area was taken for each pictures.

Mucosal polysaccharides and goblet cells were detected by Periodic acid-Schiff (PAS) staining on sections. Colons were fixed in Carnoy's solution and paraffin embedded. Slides were incubated 5 min in a solution of periodic acid 0.5%, rinsed with water and incubated 15 min in a Schiff solution. After rinsing with warm water for 5 min, slides were incubated with haematoxylin 5s, rinsed and mounted in DePeX mounting medium (SERVA). PAS-positive cells were counted along 50 full size longitudinal crypts on WT and VIVA sections obtained from three different animals per genotype.

Mucin-2 immunofluorescence staining used a specific antibody (Novusbio) revealed with a Cy3 AffiniPure Donkey Anti-Rabbit IgG (H+L). Quantification using the ImageJ software measured the mean of fluorescence on total tissue area using 10 colon sections per mouse, and 3 mice per genotype.

CoA extraction and quantification from mouse colons

Colons were flushed in Hanks' Balanced Salt Solution (HBSS)-0.25% bovine serum albumin containing phosphatase inhibitors (100 μ M suramin, 100 μ M levamisole, 1 mM sodium fluoride). Tissues were lyophilised, frozen in liquid nitrogen and dried on a SpeedVac system for 2 hours. Extraction was performed from 20 mg of a fine powder of dried colon by addition of 200 μ L of ice-cold 5% perchloric acid (in dH_2O) containing 50 μ M tris(2-carboxyethyl)phosphine (TCEP), vortexing for 15 s every 2–3 min over a 15–20 min period on ice and sonicated for 25 s. After centrifugation (10 min, 13 000 g), 50 μ L of a supernatant filtered with a 0.2 μ m syringe filter (PALL Acrodisc, 13 mm) was neutralised by adding about 45 μ L 1 M NaOH until a pH of 6.5–7.0 was reached; 30 μ L of neutralised extract was added to 36.85 μ L derivatisation mixture (68 μ M TCEP, 50 mM TRIS (pH 6.8) and 17.85 μ L 100% acetonitrile). Samples were incubated for 15 min to fully reduce disulfide. Finally, 3.15 μ L of 10 mM N-[4-(7-diethylamino-4-methyl-3-coumarinyl)phenyl] maleimide (in 100% acetonitrile) was added to bring the total volume up to 70 μ L and the total acetonitrile concentration to 30%. CoA level was determined by high-performance liquid chromatography and quantified as described.³⁰

Microbiota analysis

Genomic DNA from faeces was extracted with Mobio power soil DNA isolation kit. 16S rRNA gene variable region (V4) was amplified using barcoded (12 base) primers to tag the individual samples and sequenced using standard methods on an Illumina Miseq instrument. Sequence analysis was performed in Mothur. Metagenomic contents of microbial communities were predicted from 16S rRNA gene profiles by implementing PICRUSt. Sequences with at least 97% similarity were clustered into species operational taxonomical units (OTUs) using neighbour joining algorithm within Mothur. OTU abundance were normalised by subsampling to the lowest number of sequences within analysed groups. Per cent abundance of OTUs was log transformed to perform principal coordinate analysis.

Nuclear magnetic resonance metabolomics

Aqueous faecal extracts were prepared with 30 mg of thawed faeces in 1 mL of phosphate-buffered saline (1.9 mM Na_2HPO_4 , 8.1 mM NaH_2PO_4 , 150 mM NaCl, pH 7.4) containing 90:10 $\text{D}_2\text{O}/\text{H}_2\text{O}$ (v/v) for the field lock of the nuclear magnetic resonance (NMR) spectrometer, and 1 mM of sodium

3-(trimethylsilyl)[2,2,3,3,-2H4]propionate acting as a chemical shift reference. The mixture was homogenised, sonicated and centrifuged (18 000 g, 1 hour, 4°C). Supernatants were centrifuged again (15 000 g, 15 min, 4°C) and 600 μ L were transferred into 5 mm NMR tubes or stored at -80°C until analysis.

The NMR spectra were recorded on a 600 MHz Bruker Avance III spectrometer (Bruker Biospin, Karlsruhe, Germany) with sample temperature at 300 K. Spectra were recorded using a Carr-Purcell-Meiboom-Gill NMR sequence with a total spin echo time of 64 ms and a number of loops of 200, preceded by a water presaturation pulse during a relaxation delay of 2 s. For each spectrum, 128 free induction decays (FID) of 65 k data points were collected using a spectral width of 20 ppm with an acquisition time of 2.72 s. For all the spectra, the FIDs were multiplied by an exponential weighting function corresponding to a line broadening of 0.3 Hz and zero-filled prior to Fourier transformation. Assignments of the faecal metabolite signals were performed using 1H-1H TOCSY, 1H-13C HSQC spectra, in-house and online databases. The 1H-1D NMR spectra were exported to AMIX 3.8 software (Bruker Biospin) and divided into 0.001 ppm width buckets. The NMR dataset X-matrix (28 observations \times 8251 buckets) was normalised to the total spectrum intensity and subjected to multivariate statistical analysis using the software SIMCA-P+ V.0.14 (Umetrics, Umeå, Sweden).

Liquid chromatography-mass spectrometry metabolomics

Metabolomics profiling of faecal content of VIVA and CEA+Pan-treated WT mice was investigated by the liquid chromatography with high-resolution mass spectrometer method (ie, two chromatographic columns, in positive ionisation mode for the C18 column, and negative for the Zic-p-HILIC column) developed at CEA/SPI (Centre de Saclay, Gif-sur-Yvette, France). Mechanical lyse extraction of metabolites was done with the Precellys Soft Tissue homogenising CK14 BertinPharma and starting with 10 mg of faeces in a mixture of H_2O 20%/methanol 80%. All data processing were carried out at CEA/SPI including automatic integration of peaks, selection of relevant variables, annotation with internal databases (mz and RT) and statistical multivariate (principal component analysis-partial least square) and univariate (Wilcoxon test) analysis.

Data reproducibility and statistical analysis

All experiments were replicated and analysed independently by different experimenters at least three times. Results are expressed as means \pm SE. Statistical analysis were performed using the GraphPad Prism for Windows software. Statistical significance of the data was compared using the Student's t-test or two-way analysis of variance.

Additional methods are available as online supplemental materials.

RESULTS

High VNN1 expression correlates with IBD severity

Examination of Sanofi's Array Land database that includes multiple transcriptomic studies on larger cohorts of patients with IBD confirmed that VNN1 is highly expressed in colon biopsies from patients with IBD (figure 1A). This observation was confirmed at the single cell level where VNN1 expression was detected in colonocytes and goblet cells from patients with UC (online supplemental figure S1A). To evaluate VNN1 expression at different stages of the disease, a transcriptomic analysis was performed on colon biopsies obtained from patients with CD and UC under various therapies (online supplemental figure

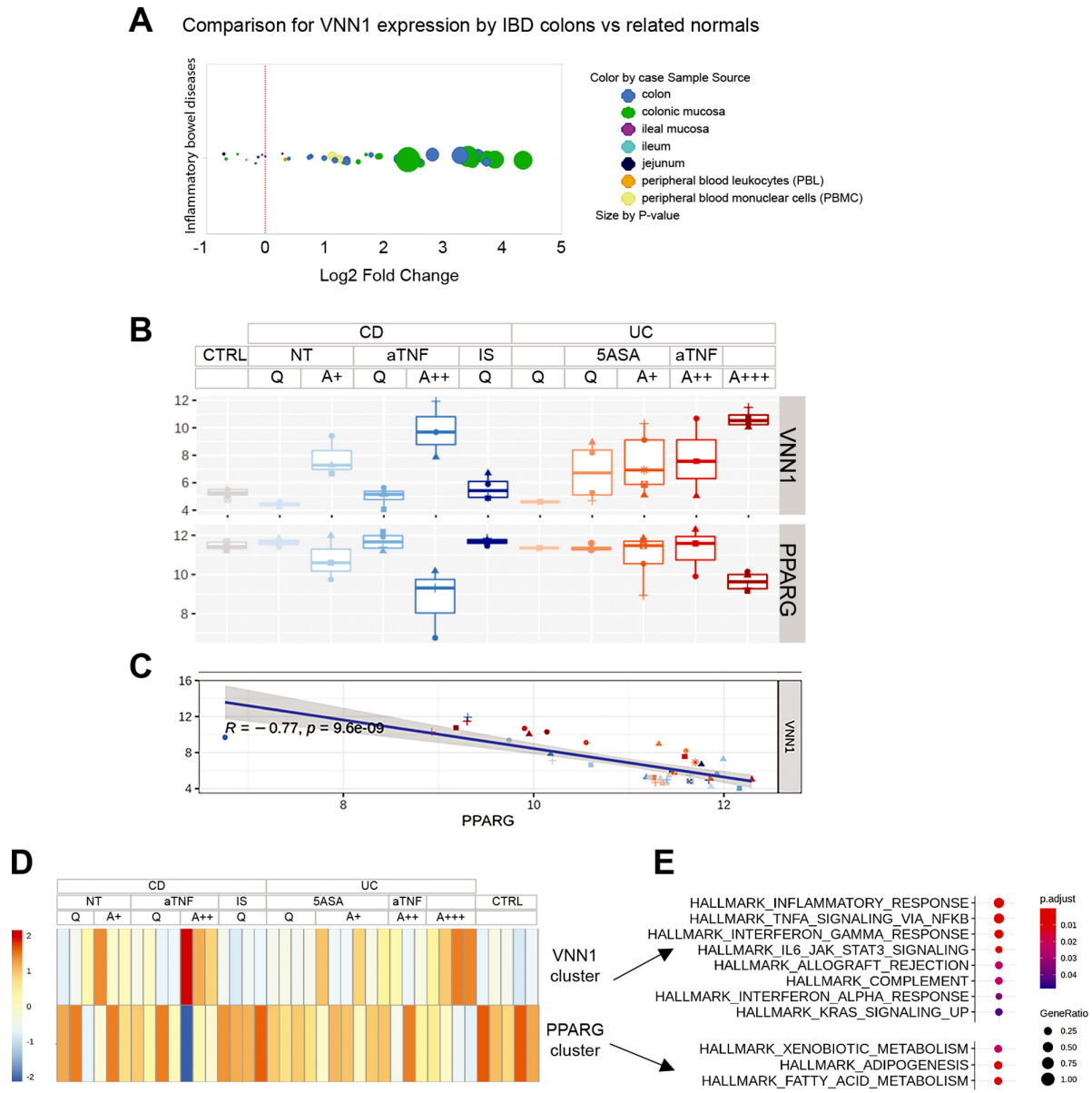


Figure 1 VNN1 is overexpressed in colonic mucosa of patients with IBD and its expression follows disease severity. (A) Schematic diagram representing an in silico study of VNN1 expression in public databases on deregulated gene sets derived from the comparisons of human IBD (UC or Crohn's disease (CD)) versus normal samples. The colour of the dot specifies the cell source of the samples; its size indicates the significance of the comparison (p value). (B) Expression of VNN1 and peroxisome proliferator-activated receptor gamma (PPAR γ) extracted from a RNA sequencing (RNAseq) analysis of colon biopsy samples isolated from patients with IBD and control (CTRL) individuals. (A, active disease; '+' indicates the clinical severity of the disease; aTNF, antitumour necrosis factor alpha biologics; 5-ASA, 5-aminosalicylic acid; IS, immunosuppressors; Nt, non-treated; Q, quiescent disease). (C) Scatter plot correlating VNN1 versus PPAR γ expression in IBD samples. (D) Description of VNN1-like and PPAR γ -like gene modules obtained from the WGCNA clustering of genes with shared expression profile across the diverse IBD samples. (E) Functional annotation of the VNN1 and PPAR γ gene modules presented in D by Ensemble of Gene Set Enrichment Analysis on the human Hallmark signature collection.

S1B, C). First, an Ensemble of Gene Set Enrichment Analysis showed that: (1) patients with active disease display a dominant cytokine-driven inflammatory signature; (2) failure of anti-TNF α biologics is associated with enhanced tissue inflammation and disorganisation; (3) clinically quiescent patients with CD show enhanced metabolic and repair signatures; (4) anti-TNF α responders lose inflammatory, metabolic and repair signatures, witnessing tissue recovery (online supplemental figure S2). We show here that VNN1 expression level parallels IBD flares and reaches the highest levels in patients resistant to anti-TNF α biologics (figure 1B, online supplemental figure S1D). In mouse, we have shown that Vnn1 is a PPAR γ target gene, and a negative

regulator of its expression and activation by pharmacological agonists.^{26 27} In IBD samples, high VNN1 expression level is associated with a decrease in peroxisome proliferator-activated receptor gamma (PPAR γ) transcripts (figure 1B and C), suggesting alterations of PPAR γ -dependent transcriptional signatures in VNN1 high patients. We used the weighted gene co-expression network analysis (WGCNA) clustering method to group genes with a similar expression profile at different stages of disease evolution (online supplemental figure S3A), and identified a module displaying a VNN1-like expression pattern (figure 1D) enriched in inflammatory and immune markers (figure 1E). PPAR γ was clustered in a distinct module functionally associated

with detoxification and lipid metabolism (figure 1E). In patients with severe IBD with low PPAR γ , the expression of target genes was reduced (online supplemental figure S3B), as observed in other colonic pathologies (online supplemental figure S3C). This includes the carnitine transporter SLC22A5 and the glucuronidation enzyme UGT1A9, suggesting that FAO and detoxification pathways might be impaired, respectively,^{31 32} whereas KLF4 and TSC22D1 reflect a more global impairment of colonocyte differentiation and polarisation.^{33 34} In contrast, other target genes including VNN1 were dissociated from PPAR γ downregulation and remain highly expressed. Thus, colonic VNN1 overexpression is associated with an inflammatory signature and severe IBD

in patients, but its precise involvement in tissue adaptation to stress remains unexplained.

Vnn1 overexpression by colonocytes confers protection to DSS-induced colitis

To mimic the situation observed in patients with IBD and explore the contribution of Vnn1 overexpression in colitis, we generated the VIVA transgenic mouse (for 'Villin-VAnin-1') in which the villin promoter drives Vnn1 overexpression in intestinal epithelial cells (online supplemental figure S4). Quantification of Vnn1 protein levels and pantetheinase activity confirmed high expression only in the gut mucosa (figure 2A; online supplemental

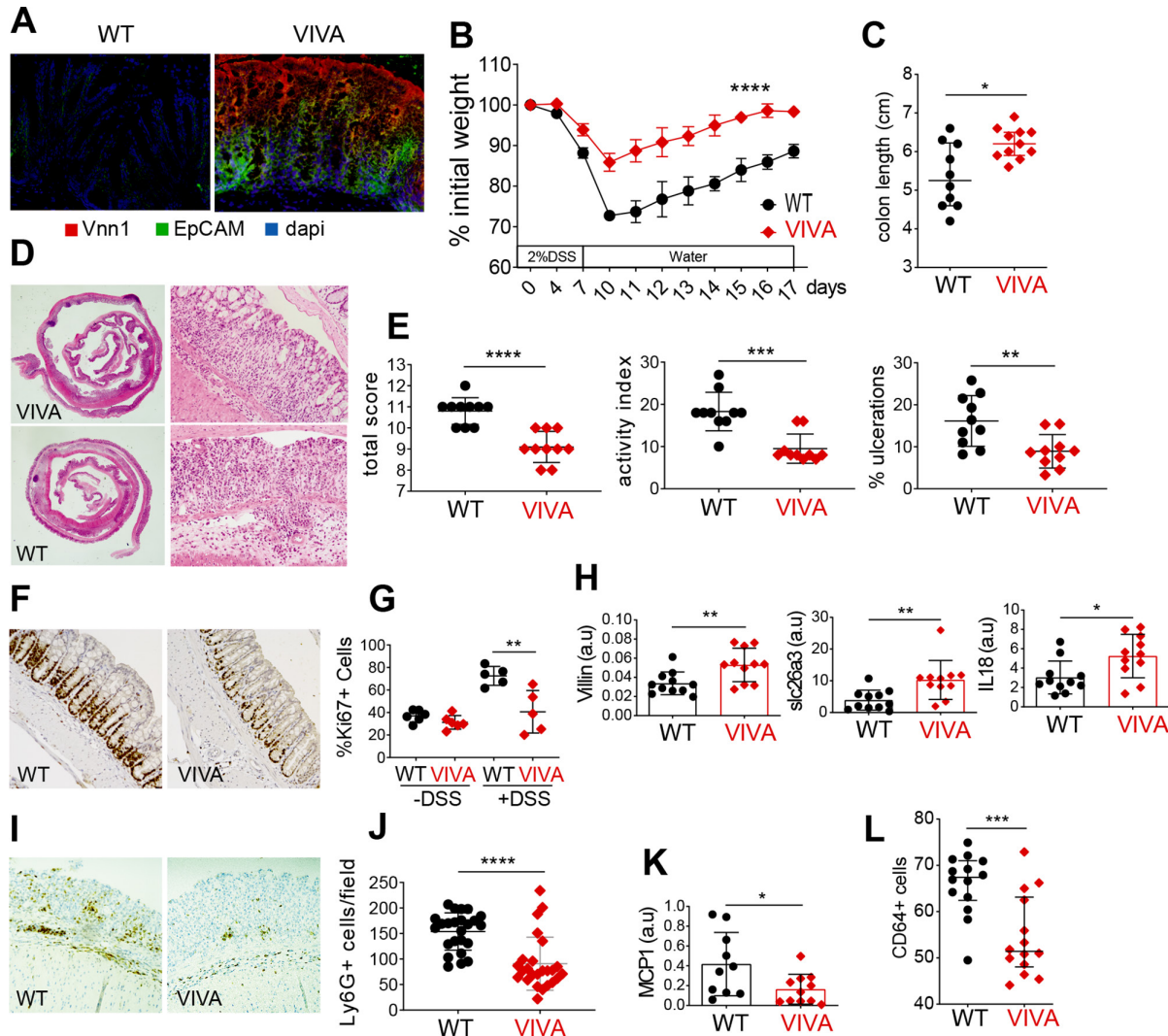


Figure 2 Vnn1 overexpression on colonocytes confers resistance to dextran sodium sulfate (DSS)-induced colitis in VIVA mice. All explorations were made at day 7 of the DSS-colitis protocol except (L). (A) Comparative expression of Vnn1 in control (wild-type (WT)) versus VIVA colons by immunofluorescence (Vnn1 (red); the epithelial marker EpCAM (green); DAPI (blue)). (B) Monitoring of total body weight loss of WT and VIVA mice during the DSS-colitis experiment (WT n=16; VIVA n=18). (C) Measurement of colon shortening (WT n=10; VIVA n=11). (D) Left panel: representative H&E staining of paraffin-embedded sections of 'swiss-roll' prepared from WT and VIVA whole colons; right panel: higher magnification focused on representative inflammatory regions. (E) Detail of the anatomopathological scoring of colitis severity between WT and VIVA mice based on swiss-roll sections examination (n=10). (F) Representative distribution of proliferating Ki67-positive cells in the crypts of WT and VIVA mucosa during DSS treatment and quantification in (G). (H) Quantitative reverse transcription-PCR (qRT-PCR) experiments showing the differential expression of epithelial markers in WT and VIVA total colon samples (n=11). (I) Immunohistochemistry using a specific anti-Ly6G antibody showing the neutrophil infiltration in ulcerative areas in WT and VIVA colons exposed to DSS and quantification in (J). (K) qRT-PCR analysis of the monocyte attractant chemokine MCP1/CCL2 in total colon samples from WT and VIVA mice exposed to DSS (n=10). (L) Percentage of lamina propria CD64+ myeloid cells found by FACS analysis in whole colons from WT and VIVA mice at day 4 of DSS (n=14). *P<0.05; **p<0.01; ***p<0.001; ****p<0.0001.

figure S4). When subjected to DSS-induced colitis, VIVA mice showed reduced weight loss (figure 2B), and colonic shortening (figure 2C) compared with DSS-fed control mice. The difference in weight persisted after DSS withdrawal during the recovery phase. At day 7 of DSS treatment, histological scoring of tissue damage and inflammation showed a higher colitis grade and activity index in colons from DSS-treated control mice when compared with VIVA mice (figure 2D–E). Inflammation was systematically coupled to ulcerative foci and crypt damage in control mice, whereas in VIVA colons areas of crypt loss without epithelial ulceration were observed. The proportion of Ki67+ cycling crypt cells was identical in both genotypes under basal conditions, but was significantly enhanced in control but not VIVA colons during colitis (figure 2F–G), suggesting compensatory epithelial cell proliferation. In contrast, expression of genes associated with epithelial functions was systematically higher in VIVA colons (figure 2H). Those include the villin, the anion transporter *slc26a3* that regulates the intracellular pH of colonocytes and whose loss is associated with colitis susceptibility,³⁵ and interleukin (IL)-18 involved in epithelial homeostasis, antimicrobial response and goblet cell function.³⁶ Neutrophil infiltration was lower in VIVA compared with controls (figure 2I–J), in agreement with the reduced degree of tissue damage in these mice. Although inflammation develops in VIVA colon, mucosal integrity is better preserved from DSS-induced damage, requiring less repair processes. The latter depend on CCL2-mediated recruitment of monocytes.³⁷ Accordingly, we observed reduced levels of MCP1/CCL2 chemokine transcripts and of infiltrating CD64+ lamina propria monocytes in VIVA colons compared with controls (figure 2K–L). No difference in other gut immunocyte subpopulations was detectable (not shown). Thus, increased *Vnn1* expression by colonocytes is associated with the preservation of the epithelial barrier and a limited development of experimental DSS-induced colitis in mice.

Improved gut barrier in VIVA mice

Using the fluorescein isothiocyanate (FITC)-dextran permeability protocol, we found a lower concentration of FITC-dextran in serum of VIVA versus control mice at day 5 of DSS (figure 3A), indicative of reduced DSS-induced increase in intestinal permeability.

Goblet cells secrete mucus glycoproteins and are often altered in IBD.³⁸ We found more PAS+ goblet cells/crypt on VIVA sections compared with WT (figure 3B–C), confirmed by PAS-coloured membrane blots (online supplemental figure S5A). Immunofluorescence on tissue confirmed the increased Muc2 staining in VIVA mice (figure 3D–E), although variable in intensity when quantified by qRT-PCR on purified colonocytes (figure 3F). Using electron microscopy, we showed that the mean values of mucus thickness were 183 nm vs 324 nm in control versus VIVA mice, respectively ($p=0.0004$) (figure 3G–H and online supplemental figure S5B). We then examined the intracellular stores of mucus by goblet cells at the base of the colonic crypts. As described, DSS induced intense secreting activity leading to mucus depletion in WT goblet cells,³⁹ a phenotype not detected in VIVA crypts (figure 3I and online supplemental figure S5C). Consequently, half of the WT but no VIVA crypts were colonised by invading bacteria (figure 3I). We also detected an increased expression of goblet cell-derived AMPs (ITLN1, ANG4, RETNLB) in VIVA mice (figure 3J). Thus, *Vnn1* overexpression is associated with enhanced production of effector proteins associated with barrier integrity.

Metabolic rewiring preserves colonocyte fitness and tolerance to stress in VIVA mice

Vnn1 contributes to vitamin B₅ and CoA homeostasis.⁴⁰ Accordingly, CoA levels are significantly elevated in VIVA colons (figure 4A). Since a shift to anaerobic glycolysis is often associated with tissue inflammation, we hypothesised that *Vnn1* might regulate the metabolic preferences in colonocytes. Given the key role of CoA in energetic metabolism and ATP-dependent processes such as protein translation, we probed the global translation rate in colon using the puromycin-based Surface Sensing of Translation method.⁴¹ We showed an increased level of puromycin staining in VIVA colons by western blot (figure 4B–C) and immunofluorescence analyses (figure 4D). Furthermore, MitoSox staining suggested that mitochondrial activity was higher in VIVA colonocytes (figure 4E–F) whereas, on stimulation with DSS, lactate production increased in control but not VIVA colonocytes (figure 4G), suggesting that the inflammation-driven glycolytic switch was antagonised.

To evaluate transcriptional changes associated with colonocyte fitness, we performed a microarray analysis of laser microdissected colon epithelial layers (online supplemental figure S6A) at basal state vs 4 days post-DSS, before the development of overt inflammation. Under basal conditions, VIVA colonocytes displayed an upregulated epithelial signature indicative of a response to trophic factors (EGF, TGF β , MAPK, Stat3) and control of cell proliferation (Hippo, Id1) (online supplemental figure S6B and figure 4H–I). We also found enrichment in a set of genes associated with responses to drugs that we previously showed to be modulated by *Vnn1* (figure 4I).^{22–24} As observed in patients with IBD, the expression of PPAR γ was inversely correlated to that of *Vnn1* (online supplemental figure S6C) but unlike that of its other target gene *SLC22A5* (online supplemental figure S6D).

On DSS exposure, control colonocytes upregulated the expression of stress-associated genes (WT_DSS_UP) (online supplemental figure S6E), also shown by GSEA to be overrepresented in samples from patients with UC or CD (figure 4J). In contrast, this signature was absent in DSS-exposed VIVA colonocytes (WT_DSS_UP against VIVA_CT vs VIVA_DSS) (figure 4J–K), where transcriptional variations mostly concerned innate immune functions, GPCR signalling, growth and metabolic regulation (figure 4L). Overall, these data argue for a global enhancement of colonocyte fitness and tissue tolerance to stress in VIVA colons.

Dysbiosis and enhanced faecal butyrate production in VIVA mice

Susceptibility to colitis depends on interactions of gut microbiota with the mucosa.⁶ On cohousing of WT and VIVA mice, the susceptibility of WT mice to DSS-colitis was reduced to a level comparable to that of VIVA mice (figure 5A). The global improvement of colitis in control mice and the preservation of a protected phenotype in VIVA mice suggest that a protective microbial community has been transferred from VIVA to control mice. We performed an analysis of the faecal microbiota in control, VIVA and *Vnn1*-deficient mice under homeostatic conditions. While a similar distribution of the main phyla was observed between the mouse groups, microbiota diversity assessed with the Shannon index was significantly reduced in VIVA (figure 5C) and bacterial composition significantly differed between groups affecting both genera and molecular species (OTUs) (figure 5B). VIVA mouse microbiota showed increased proportions of SCFAs producers *Barnesiella* and *Pseudoflavonifractor* and conversely,

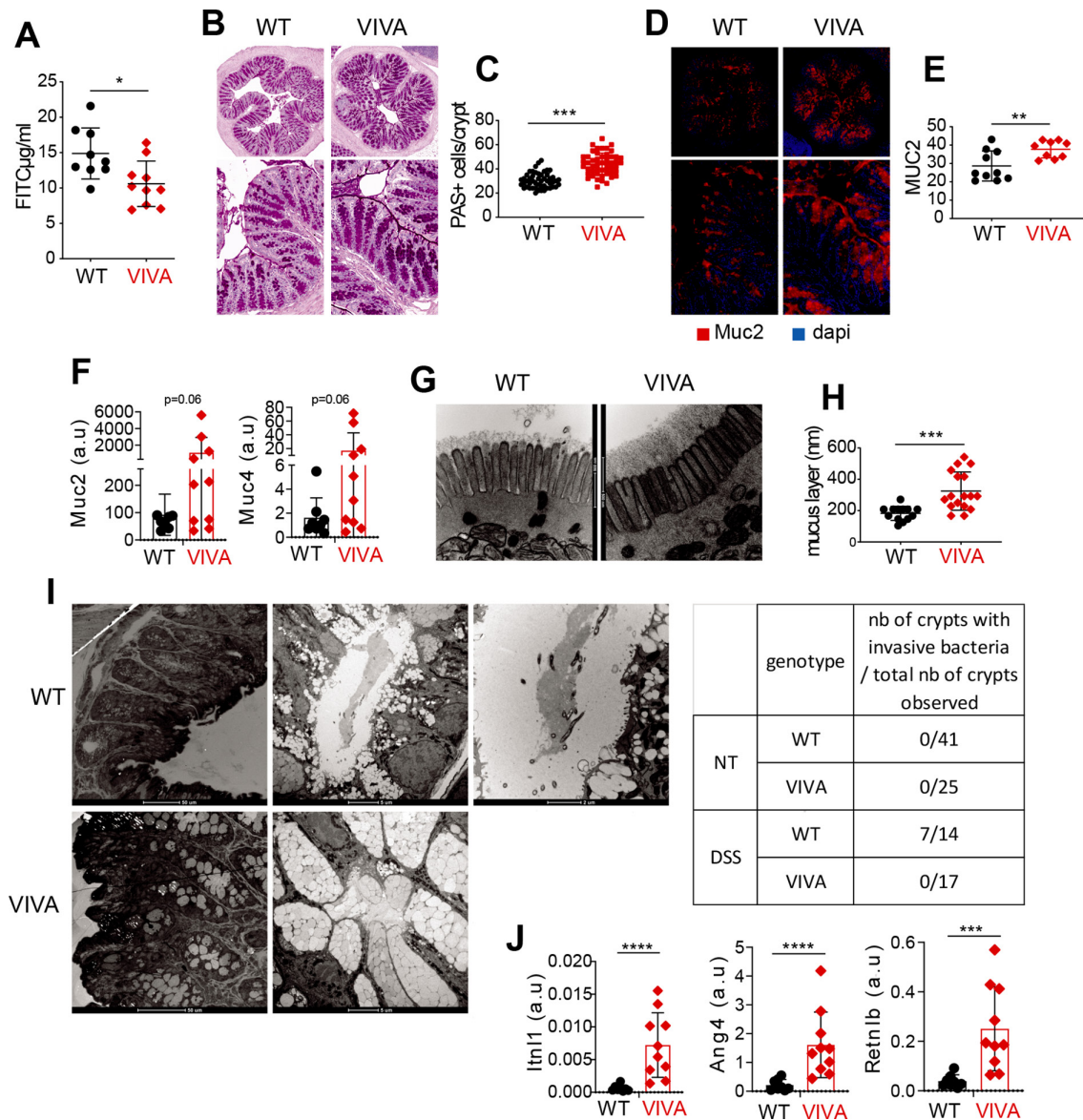


Figure 3 Improved gut barrier limits bacterial invasion of VIVA colonic crypts during dextran sodium sulfate (DSS)-colitis. (A) Mucosal permeability assessed by scoring the level of fluorescein isothiocyanate (FITC)-labelled dextran detected in blood after gavage of mice at day 4 of DSS (n=10). (B) Representative results of Periodic acid-Schiff (PAS) colourations on fixed sections of wild-type (WT) and VIVA colons, counterstained with haematoxylin (n=3). (C) Quantification of PAS-positive cells along full size longitudinal crypts on WT and VIVA colon sections (results obtained from 50 analysed crypts from three different mice per genotype). (D) Representative histological sections of immunofluorescence labelling of Muc2 (red) on WT and VIVA colonic mucosa (DAPI: blue) (n=3). (E) Quantification of the means of fluorescence of Muc2/total tissue area on 10 colon sections/mouse genotype as shown in D using the ImageJ software (n=3). (F) Quantitative reverse transcription-PCR (qRT-PCR) experiments showing the differential expression of Muc2 and Muc4 in WT and VIVA isolated colonocytes (n=10). CT values were normalised according to the expression of SPDEF as a goblet cell marker. (G) Electron microscopy analysis showing mucus accumulation at the apical surface of the colonic epithelial layer in resting conditions. Images are representative of 17 photographic shots/mouse genotype (n=3). (H) Measurement of the thickness of the mucus layer from 17 observed images as presented in G (n=3). (I) Left panel: electron microscopy analysis showing mucus accumulation and the presence of invasive bacteria at the bottom of colonic crypts in resting and DSS-treated conditions, quantified in the right panel (n=3 mice per condition). (J) qRT-PCR analysis of the expression of antimicrobial peptides from WT and VIVA isolated colonocytes in resting conditions (n=10). CT values were normalised according to the expression of SPDEF as a marker of goblet cell enrichment. *P<0.05; **p<0.01; ***p<0.001; ****p<0.0001. NT, non-treated.

decreased percentages of *Eubacterium* (figure 5D).⁴² Thus, the level of Vnn1 at the brush border of colonocytes influences the homeostasis of bacterial communities.

Microbiota exchange biological material and metabolites with the mucosa.⁴³ We thus analysed the composition of the faecal metabolome using a NMR-based metabolomic approach. Under resting conditions, Vnn1 levels influenced the respective concentrations of various metabolites leading to the segregation

of two distinct groups (VIVA vs WT control) by OPLS-DA analysis (p=0.002) (figure 5E). VIVA faecal metabolome was enriched in SCFA (acetate, butyrate and propionate) compared with that of controls (figure 5F) and this predominantly affected butyrate levels (figure 5G and online supplemental figure S7A). Butyrate is the predominant energetic resource for colonocytes and modulates intracellular signalling.⁴⁴ GSEA of VIVA versus WT samples highlighted the upregulation of a geneset

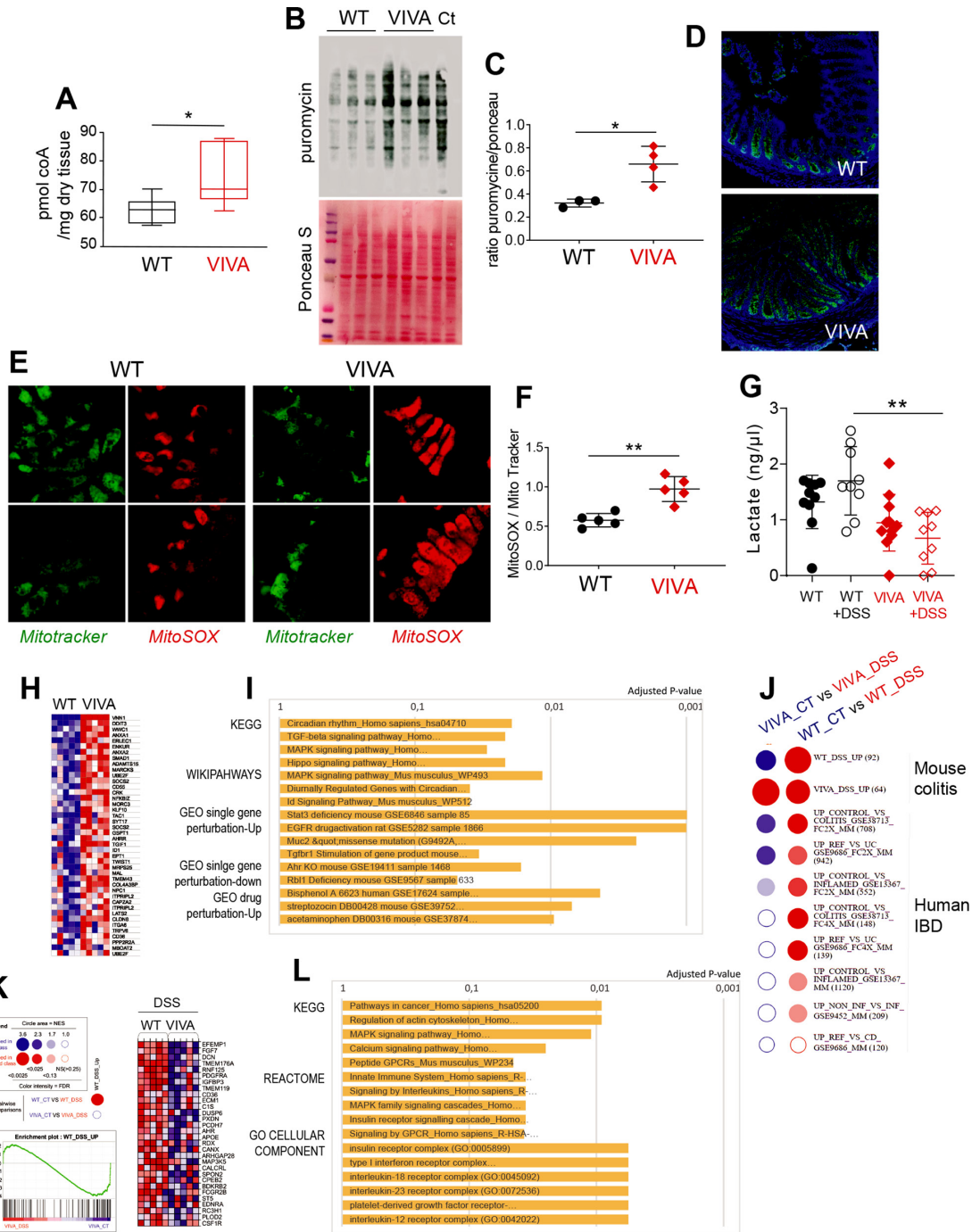


Figure 4 VIVA colonocytes display a trophic signature and improved fitness. (A) Dosage of coenzyme A (CoA) in whole colon preparations from wild-type (WT) and VIVA mice (n=7). (B) Western blot analysis of puromycin incorporation in WT (n=3) and VIVA (n=4) colons 30 min after Intraperitoneal injection of 40 nmol/g (Ct, non-injected WT control mouse). Ponceau S staining serves to verify equal loading for each sample (lower panel). (C) Quantification of the blot shown in B after normalisation of puromycin detection with Ponceau staining. (D) Immunofluorescence showing in vivo assimilation of puromycin (green) in WT and VIVA colon tissues (DAPI: blue). (E) Representative in vitro MitoSox (red) and MitoTracker (green) fluorescent labelling of isolated WT and VIVA colonocytes. (F) Quantification using the ImageJ software of the ratio between the means of fluorescence of MitoSox versus MitoTracker shown in E (n=5). (G) Dosage of lactate from isolated WT and VIVA colonocyte preparations in resting state and after 4 days of exposure to DSS (n=9). (H) Heatmap displaying the relative expression levels ranked from high (red) to low (blue) of the deregulated genes between VIVA and WT colonocytes at steady state, indicating the gene signature that is upregulated in VIVA. (I) Functional annotation of the upregulated genesets in VIVA colonocytes using the Enrichr analysis tool. (J) BubbleGUM analysis showing the enrichment of genesets on pairwise comparisons of WT and VIVA responses to DSS (d4) comparatively to each other or to human signatures in IBD. The bubble area is proportional to the normalised enrichments score (NES) calculated by Gene Set Enrichment Analysis. Colour intensity corresponds to the statistical significance of the enrichment. (K) Left panel: geneset enrichment plot showing the comparison of the genes found upregulated in WT DSS-treated mice to the VIVA non-treated versus DSS-treated mice differential gene expression; right panel: heatmap displaying of the most enriched genes (leading edge). (L) Functional annotation by Enrichr analysis comparing the WT and VIVA colonocyte gene profiles under DSS (d4). *P<0.05; **p<0.01.

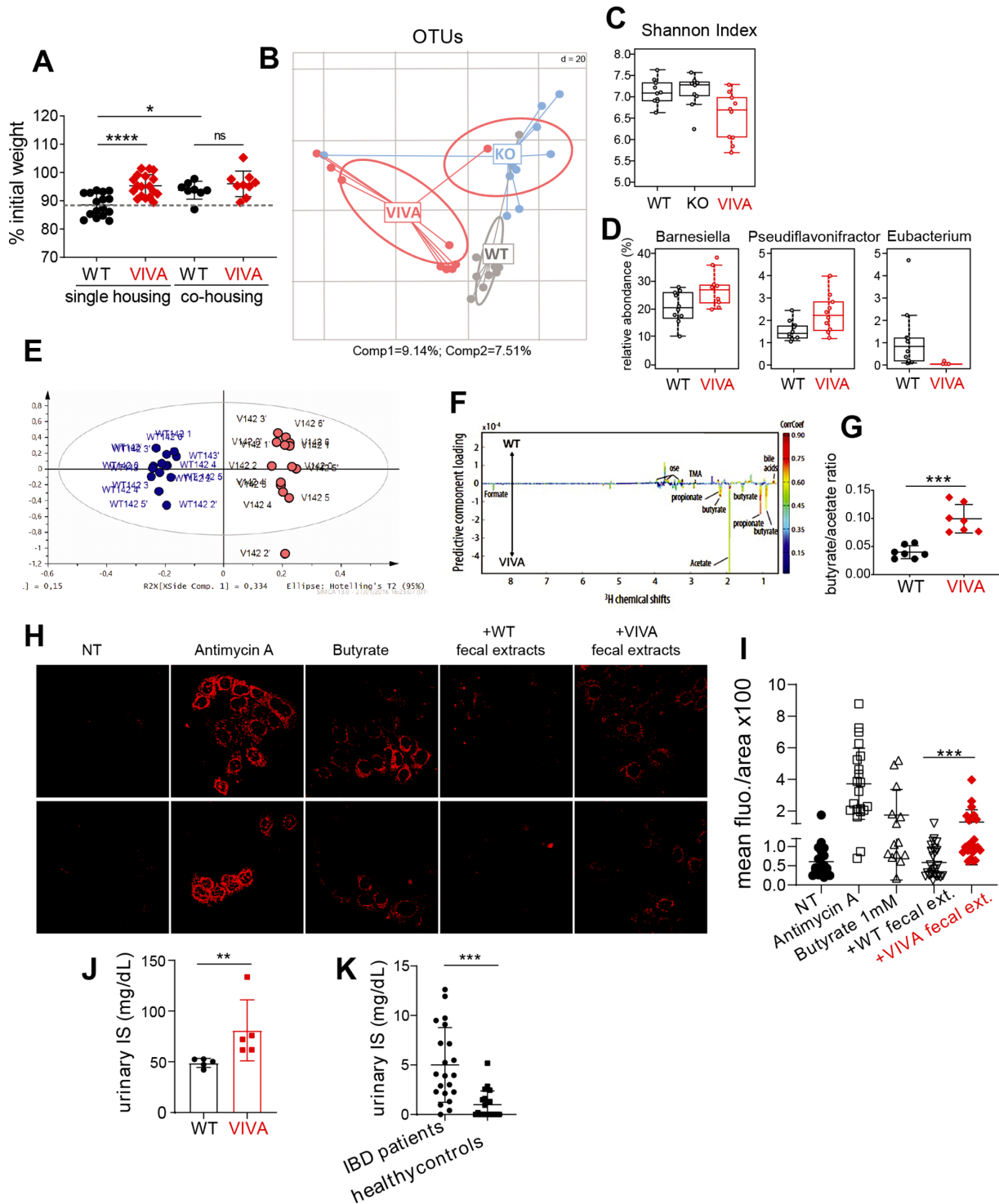


Figure 5 Overexpression of Vnn1 on gut epithelium confers changes in the microbiota composition and leads to augmented faecal levels of short chain fatty acids and indoxyl sulfate (IS). (A) Measurement of mouse weight at day 7 of dextran sodium sulfate (DSS)-colitis in co-housed (n=9) or single housed (n=18) wild-type (WT) and VIVA mice. (B) Principal component analyses of animals repartition based on their gut microbiota composition at the operational taxonomic units level (OTUs; $p=9.999e-05$) (n=10) (KO=Vnn1-deficient). (C) Box plot of the Shannon diversity index of the gut microbiota ($p<0.05$ VIVA vs KO; $p<0.05$ VIVA vs WT) (n=10). (D) Significant variations in the repartition of some bacterial strains between VIVA and WT microbiota (n=10). (E) Orthogonal partial least squares discriminant analysis (OPLS-DA) analysis revealed changes in nuclear magnetic resonance-based metabolomics profiles of VIVA compared with WT mice ($p=0.002$, analysis of variance). R2X (cum)=0.771, R2Y (cum)=0.987, Q2 (cum)=0.774 (n=14). (F) Loading plots extracted from the OPLS-DA analysis. (G) Calculated butyrate over acetate ratio in WT and VIVA faeces (n=7). (H) MitoSox fluorescent labelling of cultured Caco2 cells stimulated with butyrate supplement, or faecal extracts from WT or VIVA mice, or antimycin A as control. NT, non-treated cells. (I) Quantification of the mean of MitoSox fluorescence/area using the ImageJ software. Depending on the samples, 14–20 independent fields as shown in H were quantified. (K) Dosage of indoxyl sulfate in the urine of WT and VIVA mice. (L) Comparative measure of urinary concentrations of IS in patients with IBD (mixed Crohn's disease (CD) and UC population) versus healthy controls. * $P<0.05$; ** $p<0.01$; *** $p<0.001$; **** $p<0.0001$. ns, not significant.

associated with the response to butyrate in colonocytes (online supplemental figure S7B).⁴⁵ In vitro exposure of Caco2 cells to filtered VIVA faecal extracts provoked a higher expression of the CYP1A1 butyrate-responder gene⁴⁶ than that induced by WT controls (online supplemental figure S7C). Since butyrate feeds mitochondrial oxidative catabolism, we quantified MitROS production in Caco2 cell cultures using the MitoSox probe and found a higher fluorescent signal on contact with VIVA versus WT faecal extracts, comparable to that induced by exogenously added butyrate (figure 5H–I). Thus, the increased resistance of VIVA mice to colitis is linked to dysbiosis, enhanced butyrate levels and consequently colonocyte energetic metabolism.

Extended metabolomic profiling of faecal samples by liquid chromatography-mass spectrometry also documented an accumulation of IS in VIVA and CEA+Pan-treated WT mice (online supplemental figure S7A). The IS level was found elevated in the urine from VIVA mice and from patients with IBD (figure 5J–K).

Administration of pantetheinase metabolites recapitulates the protective phenotype in WT mice

VIVA mice constitutively express high *Vnn1* levels. This could alter gut mucosal and microbial homeostasis from birth. We tested whether preconditioning of C57BL/6 mice for 15 days prior to DSS by intraperitoneal injection of *Vnn1*-derived products CEA (120 mg/kg) and Pan (500 mg/kg) (identified as CEA+Pan therapy) would pharmacologically mimic the effect of *Vnn1* overexpression. Treated mice developed a milder colitis featuring reduced weight loss and preserved colonic length, similar to that observed in the VIVA mice (figure 6A,B). No effect was observable for treatment during the DSS protocol (online supplemental figure S8A). Whereas CEA alone had a poor influence, Pan delayed colitis development and its effect was enhanced by coadministration of CEA (online supplemental figure S8B, C). Accordingly, we observed a reduced intestinal permeability at day 4 of DSS in the treated mice (figure 6C). As in VIVA mice, CEA+Pan therapy induced the overexpression of IL-18 whereas expression of genes involved in monocyte recruitment was downregulated (online supplemental figure S8D). This treatment led to a dysbiosis (figure 6D) enriched in SCFA producers (*Odoribacter*, *Pseudoflavonifractor*) previously shown to be reduced in patients with IBD,^{42–47} and impoverished in bacterial species (*Prevotella*) associated with susceptibility to colitis (figure 6E).⁴⁸ Faecal NMR analysis performed during the time course of CEA+Pan therapy also documented a progressive increase in butyrate over acetate concentrations (figure 6F) as in VIVA faeces (figure 5G). Thus, the pharmacological administration of pantetheinase products recapitulates the mechanisms of protection against colitis conferred by *Vnn1* overexpression.

We then depleted the mouse microbiota with antibiotics, known to aggravate DSS-colitis,⁴⁹ and applied CEA+Pan therapy during the period of microbiota restoration to test whether it could recondition a protective environment. CEA+Pan-treated mice displayed an enhanced protection against colitis (online supplemental figure S8E) in favour of our hypothesis of improved microbiota resilience. In contrast, lack of *Vnn1* worsens the severity of DSS-colitis in C57BL/6 mice (online supplemental figure S8F). Administration of pantethine, a stable dimeric form of the *Vnn1* substrate PanSH, enhanced tolerance to DSS-colitis only when a functional *Vnn1* was present, that is, in WT but not *Vnn1*-deficient mice (figure 6G and online supplemental figure S8G), confirming that the enzymatic activity of *Vnn1* is mandatory for the protection.

The beneficial effect of the combined supply in CEA and Pan was also validated in the TNBS-induced colitis model (figure 6H–K). In addition, when exposed to TNBS, VIVA mice developed an attenuated colitis (online supplemental figure S9A–D). Although weight loss was equivalent in all mice in the early phase of the disease (online supplemental figure S9A), they did not exhibit clinical signs of sickness (rough coat, diarrhoea and prostration) observed in WT mice. Furthermore, the morphology of VIVA colons was better preserved, a phenotype confirmed by the lower level of cytokine/enzyme transcripts associated with acute inflammation (online supplemental figure S9B–D).

Hence, *Vnn1* or pantetheinase-associated metabolites reinforce colon homeostasis and resistance to colitis by regulating microbial ecology and maintaining butyrate-dependent energy production in colonocytes.

Vnn1 interacts with the NLRP6 inflammasome pathway

VIVA mice showed increased IL-18 secretion in the intestinal mucosa (figure 2H) and low faecal levels of the mucin-degrader *Akkermansia muciniphila* (not shown), which may result from the CEA-derived generation of taurine.⁵⁰ This metabolite has been proposed as a regulator of the NLRP6 inflammasome activity,⁵¹ which controls the colonisation of *A. muciniphila* through the production of IL-18.⁵² Thus, we applied the CEA+Pan treatment to NLRP6-deficient mice prior to DSS exposure, and found that it did not protect against DSS-induced colitis (online supplemental figure S9E–H), suggesting a role for the NLRP6 pathway in the *Vnn1*-dependent regulation of gut bacterial ecology and protection to experimental colitis.

Vnn1 is induced by inflammatory stress to cope with mucosal injury

We used a model of chronic colitis that better recapitulates the situation observed in patients with IBD, by subjecting mice to two cycles of exposure to low doses of DSS (0.75%) for longer periods of time (16 days) over 48 days. In this model of attenuated colonic inflammation, VIVA mice were still protected during inflammatory flares (figure 6L). Surprisingly, control mice developed an attenuated colitis during the second cycle of DSS induction. Since *Vnn1* is stress-inducible, we monitored faecal *Vnn1* using an ELISA and documented an increase in *Vnn1* levels during the first inflammatory cycle, which was maintained at a level comparable to that observed in VIVA mice during the second cycle. This suggests that *Vnn1* induction to tissue stress is part of a tissue adaptation process leading to a better intestinal tolerance to the pathology.

To mirror the situation of patients, WT and VIVA colon organoids were exposed to TNF for 3 days, then withdrawn to mimic a targeted anti-TNF immuno-intervention. Mucosal reconstitution was examined 2 days post-TNF removal, comparing organoids treated or not with pantethine, the substrate of *Vnn1* activity. As a result, pantethine significantly reduced the mortality rate after TNF exposure (online supplemental figure S11). Interestingly, cell death was reduced in VIVA compared with WT organoids, and addition of pantethine almost completely abolished this mortality. In all organoids, the reconstitution phase was correlated with an increase in the expression of epithelial genes such as *Muc2* and the AMP *Ang4*, which was further enhanced by addition of pantethine (online supplemental figure S11). In conclusion, the organoid experiments recapitulate the pantetheinase-dependent cytoprotective effect on epithelial cells.

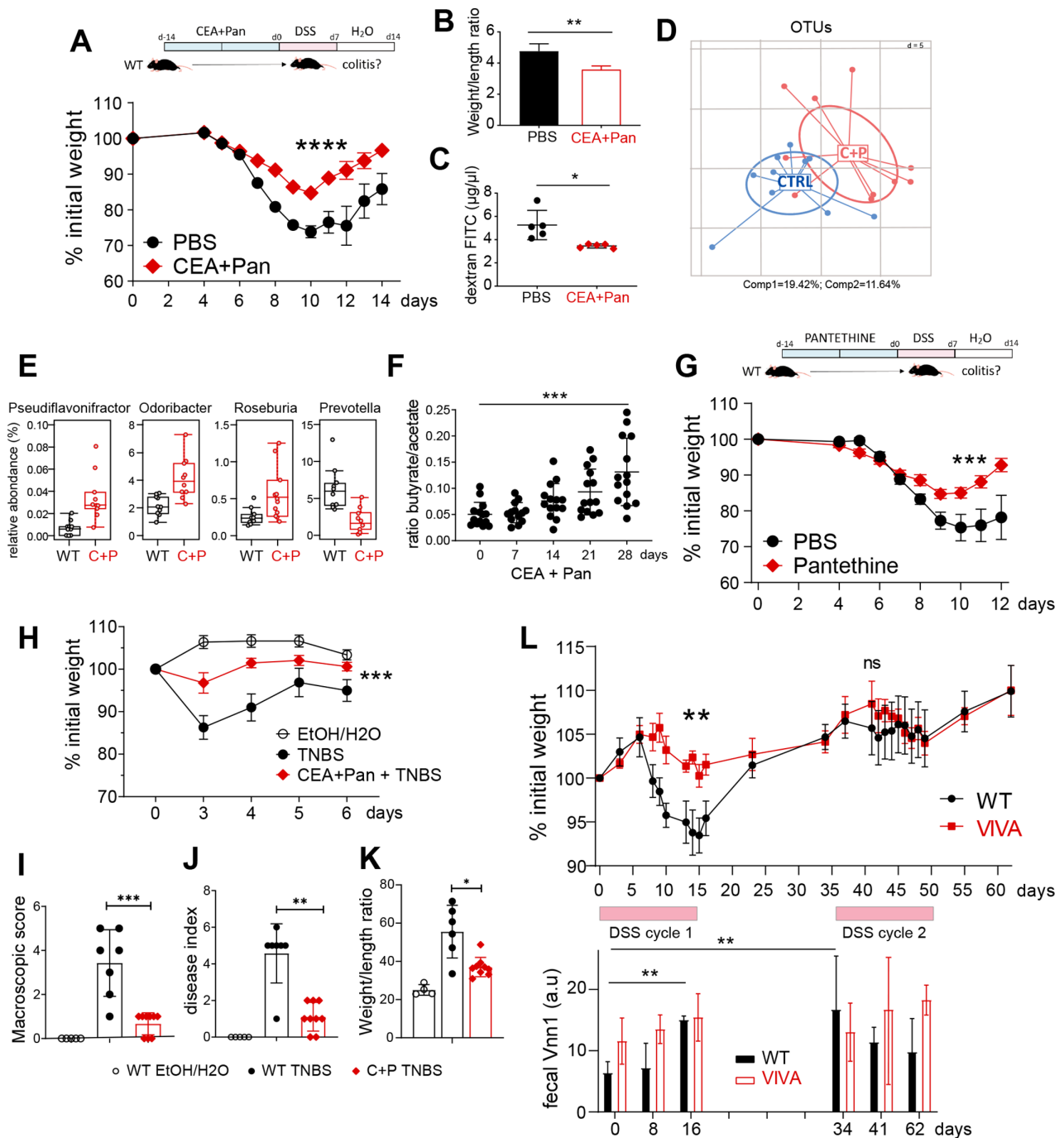


Figure 6 Supplementation of wild-type (WT) mice with Vnn1-pantetheinase substrate or products recapitulates the VIVA phenotype. (A) Upper panel: diagram representing the protocol used for the combined treatment with pantothenic acid (Pan) plus cysteamine (CEA), and induction dextran sodium sulfate (DSS)-colitis in WT mice. Lower panel: monitoring of the total body weight loss in pretreated (CEA+Pan) or non-treated control (phosphate buffered saline (PBS)) WT mice during DSS-colitis (n=20). (B) Measurement of colon shortening at day 11 of the DSS-colitis protocol (n=5). (C) Mucosal permeability assessed by scoring of the level of fluorescein isothiocyanate (FITC)-labelled dextran retrieved in blood after gavage of mice at day 4 of DSS (n=5). (D) Principal component analyses of animals repartition based on their gut microbiota composition at the operational taxonomic units level (OTUs; $p=9.999e-05$) (n=10). (E) Variations in the repartition of some microbiota bacterial strains between non-treated (WT) and CEA+Pan-treated (C+P) mice (n=10). (F) Evolution of the butyrate over acetate ratio over time during CEA+Pan treatment (n=14). (G) Upper panel: diagram representing the protocol used for the treatment with pantethine and induction DSS-colitis in WT mice. Lower panel: monitoring of weight loss in pantethine-treated and untreated mice (PBS) during DSS-colitis (n=5). (H) Monitoring of the total body weight loss in pretreated (CEA+Pan) or non-treated WT mice during 2,4,6-trinitrobenzene sulfonic acid (TNBS)-colitis. Control mice received intrarectal administration of EtOH/H₂O. (I) Macroscopic assessment of the colitis grade was scored according to a previously reported scoring system (Bell⁵⁸ 1995). (J) The disease activity index (DAI) was calculated as the total of the scores: the sum of weight loss, diarrhoea and bleeding. (K) Measurement of colon shortening at day 6 of the TNBS-colitis protocol. (L) Upper panel: monitoring of weight loss in WT and VIVA mice during repeated cycle of low DSS (0.75%) (n=5). Lower panel: dosage by ELISA of Vnn1 in faeces during the DSS cycles (n=5). * $P<0.05$; ** $p<0.01$; *** $p<0.001$; **** $p<0.0001$. ns, not significant.

We then tested whether the reduction in PPAR γ expression associated with high *Vnn1* expression could constitute an additional aggravating factor. Addition of the PPAR γ agonist rosiglitazone to WT or VIVA organoids reduced TNF-mediated cell death; in contrast supplying the PPAR γ antagonist Bisphenol A diglycidyl ether (BADGE) partially abrogated the protective effect of pantetheine (online supplemental figure S11). Under these conditions, *Muc2* or *Ang4* expression levels were not affected.

DISCUSSION

Our work established that colonic expression of *VNN1* is highly induced in IBD and follows disease severity and unresponsiveness to therapy. *VNN1* has been identified as a biomarker in several inflammatory disorders in human,^{25 27 53–55} but its contribution to gut inflammation is still unresolved. In mouse, our former studies performed in *Vnn1*-deficient BALB/c animals showed that *Vnn1* was a regulator of glutathione (GSH) levels in the liver and PPAR γ activation in the colon,^{21 26} and exerted a proinflammatory role.^{24 26 28} These studies used a systemic knockout of the *Vnn1* gene that was able to affect all tissues throughout mouse development. Indeed, the lack of *Vnn1* in BALB/c mice normalised GSH levels in the liver to a level comparable to that of WT C57BL/6 mice, thereby explaining in part the proinflammatory role of *Vnn1* in gut inflammatory models in the BALB/c background. We show here that *Vnn1*-deficient C57BL/6 mice are more susceptible to DSS-colitis than control mice and that *Vnn1* expression contributes to the colonocyte cytoprotection, a phenotype also observed in the islets of non-obese diabetic (NOD) mice.²³ Hence, mouse context modulates the effect of variations in *Vnn1* levels on the balance between cytoprotection and inflammation.

To explore the role of *Vnn1* overexpression in inflamed gut mucosa, we developed the transgenic VIVA model. At basal stage, *Vnn1* overexpression by colonocytes enhanced growth-associated transcriptional profiles suggestive of increased fitness, attested by the level of mucus and AMP production and the control of permeability. Therefore, VIVA mice are less susceptible to experimental colitis models. Most changes were observed early after the induction of colitis, before the development of acute inflammation. Consequently, DSS-treated VIVA crypts remained bacteria-free for longer periods and the mucosal barrier is protected from the translocation of bacteria where they trigger inflammation.

Vnn1 is the predominant mouse tissue pantetheinase that hydrolyses PanSH into CEA and Pan (vitamin B₅), the precursor of CoA synthesis.¹⁹ As seen in a tumour model,⁴⁰ we demonstrate that the level of *Vnn1* on colonocytes parallels that of CoA in gut tissue. CoA plays a major role in FAO and OXPHOS. Mitochondrial activity and protein translation were augmented in VIVA mice and, under inflamed conditions, *Vnn1* overexpression prevented the inflammation-associated glycolytic shift. This effect could also be due to CEA, shown to partially inhibit glycolytic enzymes.⁴⁰ The efficacy of FAO and OXPHOS critically depends on fatty acid substrates, particularly if glycolysis is reduced. Butyrate, produced by the fermentative metabolism of several bacterial species in the microbiota, is a main source of colonic SCFA.⁵⁰ VIVA mice display a dysbiosis enriched in SCFA-producing bacterial species often under-represented in IBD. Increase in faecal butyrate levels boosted the transcription of butyrate target genes in cultured colonocyte cell lines. Although other changes in the faecal metabolome cannot be formally excluded, *Vnn1* induces a potent synergic effect between butyrate production by microbiota and increased CoA-dependent FAO

and OXPHOS in colonocytes. This virtuous energetic loop may explain their improved fitness and function.

High *Vnn1* expression was also associated with an increased detection of IS in faeces. Measure of IS urinary concentrations is employed as surrogate of changes in the gut microflora indicating expansion of bacterial species exploiting tryptophan fermentation. In most patients with IBD tested, IS levels were significantly augmented suggesting that IS concentration could be exploited as a relevant marker in their follow-up.

Of major interest, we could demonstrate that co-administration of the products of *Vnn1* activity (ie, Pan and CEA) to normal mice recapitulated most of the protective phenotypes conferred by the overexpression of *Vnn1* in VIVA mice. This has been shown in both DSS-induced and TNBS-induced colitis models. Significantly, oral administration of pantethine, the substrate of *Vnn1* activity, leads to the same protective result but only if *Vnn1* is present, confirming the absolute requirement for this enzymatic activity. CEA+Pan-treated mice display an enrichment in SCFA-producers and faecal butyrate, and showed improved microbial resilience after antibiotic therapy *in vivo*. This demonstrates that *Vnn1* products can modulate the microbial ecology at the luminal surface of the gut and favour growth and/or fermentative activity of particular bacteria. Interestingly, the CEA+Pan supply did not protect the NLRP6-deficient mice from colitis. NLRP6 is regulated by PPAR γ and the NLRP6 inflammasome regulates IL-18 production, goblet cell function and microbiome composition in the intestine. In addition, CEA is a major precursor of taurine,⁵⁰ a sulfur metabolite, which has been shown to contribute to activation of the NLRP6 inflammasome. Our results suggest that the NLRP6 signalling may be involved in the *Vnn1*-pantetheinase pathway. Additional investigations would be required to study this process.

To explore a therapeutic effect, we treated mice exposed to DSS with CEA+Pan during colitis but did not observe any improvement due to the treatment under the conditions tested. Although further investigations would be needed, our interpretation is that a preconditioning of the microbiota before the initiation of the colitis is required to allow metabolic adaptation of the mucosa and tissue repair. Once colitis is established, the dampening of inflammation (eg, anti-TNF treatment) is required to allow CEA+Pan-dependent mucosal restoration.

Our results argue that *Vnn1* expression by colonocytes promotes microbial adaptation to beneficial SCFA-producing bacterial strains, probably through the delivery of Pan and CEA to the colonic lumen. This is associated with reduced diversity in the faecal microbiota, which is generally considered as detrimental. Under physiological conditions, high colonic expression of *Vnn1* is not observed. While the *Vnn1*-driven enrichment in SCFA-producing strains confers a significant improvement in tolerance to colitis, it might not recapitulate the benefits of a normal microbiota under unchallenged conditions. In favour of this hypothesis, we observed that VIVA mice gain less weight than control mice during their development (not shown).

Overall, these results raise an apparent paradox when comparing mouse and human data. In patients with IBD, the highest levels of *VNN1* expression correlate with severe disease and often resistance to TNF α biologics, probably as a compensatory mechanism. This hypothesis is based on the cytoprotective effect conferred by the pantetheinase activity of *Vnn1*, as demonstrated in VIVA mice and TNF-treated colonic organoids. Increased pantetheinase activity also impacts the composition of microbial communities and butyrate production, a PPAR γ activator.

We interpret the human/mouse discrepancy as follows: under physiological conditions, food and microbiota provide an appropriate supply in CEA and Pan. In severe IBD, this metabolic environment becomes progressively impoverished, and the high induction of VNN1 is no longer protective due to the reduced supply of substrate. Santoru *et al* have reported a Pan deficit in patients with UC and CD,⁵⁶ and this observation was replicated in another multi-omics study.⁵⁷ In support of this interpretation, we showed that addition of pantethine to VIVA organoids further enhanced cytoprotection and/or repair potential. In a durable inflammatory context, Vnn1-dependent protection becomes insufficient, and this could be due to the significant reduction in PPAR γ expression observed in some patients, a phenotype induced by Vnn1 overexpression in mouse.²⁶ Therefore, combining anti-TNF therapy with pantetheinase derivatives should help to sustain intestinal mucosa recovery.

Author affiliations

¹Centre d'Immunologie de Marseille Luminy, Aix Marseille Université, Centre National de la Recherche Scientifique, Institut National de la Santé et de la Recherche Médicale, Marseille, France
²Department of Medicine, Brigham & Women's Hospital, Harvard Medical School, Boston, Massachusetts, USA
³Gastroenterology, AP-HM Hôpital Nord, Aix Marseille Université, Marseille, France
⁴Centre d'Investigation Clinique (CIC), AP-HM Hôpital Nord, Aix-Marseille Université, Marseille, France
⁵Genetic Mechanisms of Disease Laboratory, The Francis Crick Institute, London, UK
⁶Inserm U1019 Team 7, Inserm, Lille, France
⁷ISM2, Aix Marseille Université, Centre National de la Recherche Scientifique, Centrale Marseille, Marseille, France
⁸Stellenbosch University, Stellenbosch, Western Cape, South Africa
⁹MICALIS—UMR1319, INRA, Jouy-en-Josas, France
¹⁰Department of Gastroenterology, Inserm NGERE U1256, University Hospital of Nancy, University of Lorraine, Vandoeuvre-lès-Nancy, France

Twitter Achille Broggi @achillebro

Acknowledgements We thank Guillaume Charbonnier for his work in the bioinformatics processing of RNAseq data from the human IBD biobank. We thank Dr Caroline Laprie for her expert work as a veterinary pathologist on colitis in mice. We also thank Nicolas Brouilly from the electron microscopy platform at the IBDML in Marseille. We thank Jean Charles Martin and Catherine Tardivel for LC-MS analysis of human fecal samples on the BIOMET platform (Aix Marseille University). We thank Dr Lee Leserman for critical reading of the manuscript.

Contributors Data curation, formal analysis, investigation and methodology: VM, TG, MMal. Formal analysis and methodology: CB, CP, SC, LC, TPVM, JJM-G. Investigation and methodology: MS, NL, J-CG, ES, PL, MC, MMas, LS, KM, LP-B. Conceptualisation, formal analysis, supervision, funding acquisition, validation, investigation, methodology, project administration, writing original draft, review and editing: PN, FG. Guarantor: FG.

Funding TG and MMal were recipients of a doctoral contract from Aix-Marseille University. KM was supported by a doctoral bursary from the South African National Research Foundation. JJM-G was a recipient of a postdoctoral fellowship from the Fondation Pour la Recherche Médicale (FRM). Financial resources originated from institutional funding from CNRS, INSERM, AMU and APHM. This project benefited from a FRM grant (Equipe FRM DEQ20140329532) and Inserm-Transfer COPOC (n°: R19020AS), and was supported by SANOFI in the I2HD collaborative scientific programme between CIML and SANOFI (Aviesan n° 10756A10). This work was also supported by European Union under the European Regional Development Fund (MP0009273—EIRC Synchrohé) that was granted to MC.

Competing interests None declared.

Patient and public involvement Patients and/or the public were not involved in the design, or conduct, or reporting, or dissemination plans of this research.

Patient consent for publication Not applicable.

Ethics approval All experiments were performed in accordance with institutional guidelines for animal care and use. This experimental design was authorised by the Ethical Committee for Animal Experimentation (no. 02820.03). This study was approved by ClinicalTrials.gov Identifier: NCT02304666. Participants gave informed consent to participate in the study before taking part.

Provenance and peer review Not commissioned; externally peer reviewed.

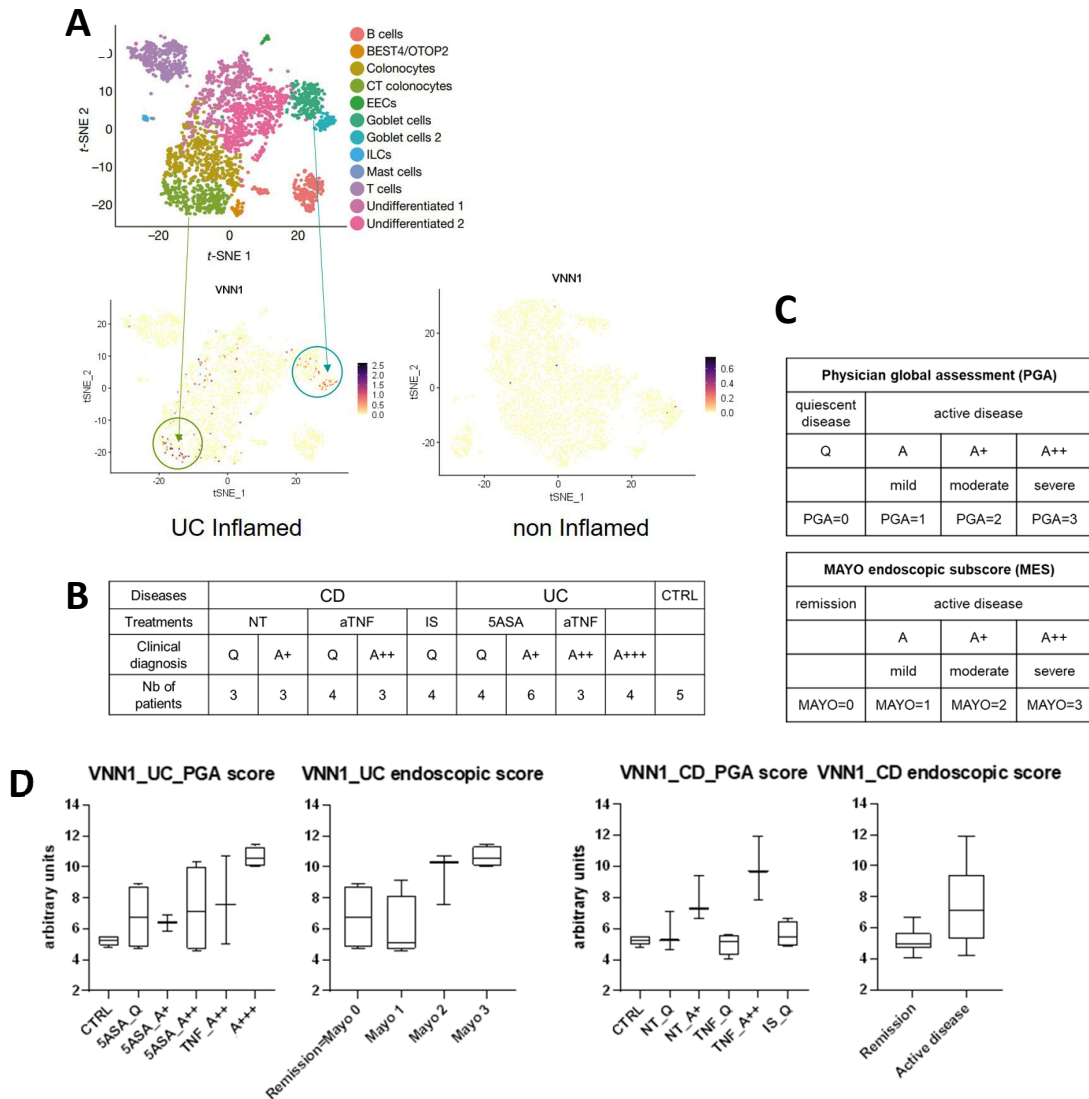
Data availability statement Data are available in a public, open access repository. All data relevant to the study are included in the article or uploaded as supplementary information.

Supplemental material This content has been supplied by the author(s). It has not been vetted by BMJ Publishing Group Limited (BMJ) and may not have been peer-reviewed. Any opinions or recommendations discussed are solely those of the author(s) and are not endorsed by BMJ. BMJ disclaims all liability and responsibility arising from any reliance placed on the content. Where the content includes any translated material, BMJ does not warrant the accuracy and reliability of the translations (including but not limited to local regulations, clinical guidelines, terminology, drug names and drug dosages), and is not responsible for any error and/or omissions arising from translation and adaptation or otherwise.

REFERENCES

- Kaser A, Zeissig S, Blumberg RS. Inflammatory bowel disease. *Annu Rev Immunol* 2010;28:573–621.
- Kaplan GG, Windsor JW. The four epidemiological stages in the global evolution of inflammatory bowel disease. *Nat Rev Gastroenterol Hepatol* 2021;18:56–66.
- Papamichael K, Lin S, Moore M, *et al*. Infliximab in inflammatory bowel disease. *Ther Adv Chronic Dis* 2019;10:2040622319838443.
- Billmeier U, Dieterich W, Neurath MF, *et al*. Molecular mechanism of action of anti-tumor necrosis factor antibodies in inflammatory bowel diseases. *World J Gastroenterol* 2016;22:9300–13.
- Chudy-Onwugaje KO, Christian KE, Farray FA, *et al*. A state-of-the-art review of new and emerging therapies for the treatment of IBD. *Inflamm Bowel Dis* 2019;25:820–30.
- Plichta DR, Graham DB, Subramanian S, *et al*. Therapeutic opportunities in inflammatory bowel disease: mechanistic dissection of Host-microbiome relationships. *Cell* 2019;178:1041–56.
- Battat R, Duijvestein M, Guizzetti L, *et al*. Histologic healing rates of medical therapies for ulcerative colitis: a systematic review and meta-analysis of randomized controlled trials. *Am J Gastroenterol* 2019;114:733–45.
- Dal Buono A, Roda G, Argollo M, *et al*. Histological healing: should it be considered as a new outcome for ulcerative colitis? *Expert Opin Biol Ther* 2020;20:407–12.
- Gupta A, Yu A, Peyrin-Biroulet L, *et al*. Treat to target: the role of histologic healing in inflammatory bowel diseases: a systematic review and meta-analysis. *Clin Gastroenterol Hepatol* 2021;19:1800–13.
- Shah SC, Colombel J-F, Sands BE, *et al*. Systematic review with meta-analysis: mucosal healing is associated with improved long-term outcomes in Crohn's disease. *Aliment Pharmacol Ther* 2016;43:317–33.
- Odenwald MA, Turner JR. The intestinal epithelial barrier: a therapeutic target? *Nat Rev Gastroenterol Hepatol* 2017;14:9–21.
- Vancamelbeke M, Vanuytsel T, Farré R, *et al*. Genetic and transcriptomic bases of intestinal epithelial barrier dysfunction in inflammatory bowel disease. *Inflamm Bowel Dis* 2017;23:1718–29.
- Allaire JM, Crowley SM, Law HT, *et al*. The intestinal epithelium: central coordinator of mucosal immunity. *Trends Immunol* 2018;39:677–96.
- Pisani LF, Moriggi M, Gelfi C, *et al*. Proteomic insights on the metabolism in inflammatory bowel disease. *World J Gastroenterol* 2020;26:696–705.
- Smillie CS, Biton M, Ordovas-Montanes J, *et al*. Intra- and Inter-cellular rewiring of the human colon during ulcerative colitis. *Cell* 2019;178:714–30.
- Litvak Y, Byndloss MX, Bäumlér AJ. Colonocyte metabolism shapes the gut microbiota. *Science* 2018;362. doi:10.1126/science.aat9076. [Epub ahead of print: 30 Nov 2018].
- Donohoe DR, Garge N, Zhang X, *et al*. The microbiome and butyrate regulate energy metabolism and autophagy in the mammalian colon. *Cell Metab* 2011;13:517–26.
- Naquet P, Kerr EW, Vickers SD, *et al*. Regulation of coenzyme A levels by degradation: the 'Ins and Outs'. *Prog Lipid Res* 2020;78:101028.
- Naquet P, Pitari G, Dupré S, *et al*. Role of the Vnn1 pantetheinase in tissue tolerance to stress. *Biochem Soc Trans* 2014;42:1094–100.
- Pitari G, Malergue F, Martin F, *et al*. Pantetheinase activity of membrane-bound Vanin-1: lack of free cysteamine in tissues of Vanin-1 deficient mice. *FEBS Lett* 2000;483:149–54.
- Berruyer C, Martin FM, Castellano R, *et al*. Vanin-1/- mice exhibit a glutathione-mediated tissue resistance to oxidative stress. *Mol Cell Biol* 2004;24:7214–24.
- Ferreira DW, Goedken MJ, Rommelaere S, *et al*. Enhanced hepatotoxicity by acetaminophen in Vanin-1 knockout mice is associated with deficient proliferative and immune responses. *Biochim Biophys Acta* 2016;1862:662–9.
- Roisin-Bouffay C, Castellano R, Valéro R, *et al*. Mouse Vanin-1 is cytoprotective for islet beta cells and regulates the development of type 1 diabetes. *Diabetologia* 2008;51:1192–201.

- 24 Martin F, Penet M-F, Malergue F, *et al.* Vanin-1(-/-) mice show decreased NSAID- and Schistosoma-induced intestinal inflammation associated with higher glutathione stores. *J Clin Invest* 2004;113:591–7.
- 25 Kaviani N, Mehlal S, Marut W, *et al.* Imbalance of the Vanin-1 pathway in systemic sclerosis. *J Immunol* 2016;197:3326–35.
- 26 Berruyer C, Pouyet L, Millet V, *et al.* Vanin-1 licenses inflammatory mediator production by gut epithelial cells and controls colitis by antagonizing peroxisome proliferator-activated receptor gamma activity. *J Exp Med* 2006;203:2817–27.
- 27 Gensollen T, Bourges C, Rihet P, *et al.* Functional polymorphisms in the regulatory regions of the VNN1 gene are associated with susceptibility to inflammatory bowel diseases. *Inflamm Bowel Dis* 2013;19:2315–25.
- 28 Pouyet L, Roisin-Bouffay C, Clément A, *et al.* Epithelial Vanin-1 controls inflammation-driven carcinogenesis in the colitis-associated colon cancer model. *Inflamm Bowel Dis* 2010;16:96–104.
- 29 Normand S, Delanoye-Crespin A, Bressenot A, *et al.* Nod-Like receptor pyrin domain-containing protein 6 (NLRP6) controls epithelial self-renewal and colorectal carcinogenesis upon injury. *Proc Natl Acad Sci U S A* 2011;108:9601–6.
- 30 Goosen R, Strauss E. Simultaneous quantification of coenzyme A and its salvage pathway intermediates in in vitro and whole cell-sourced samples. *RSC Adv* 2017;7:19717–24. doi:10.1039/C7RA00192D
- 31 Juraszek B, Nałecz KA. Slc22A5 (OCTN2) carnitine Transporter-Indispensable for cell metabolism, a Jekyll and Hyde of human cancer. *Molecules* 2019;25. doi:10.3390/molecules25010014. [Epub ahead of print: 19 Dec 2019].
- 32 Mizuma T. Intestinal glucuronidation metabolism may have a greater impact on oral bioavailability than hepatic glucuronidation metabolism in humans: a study with raloxifene, substrate for UGT1A1, 1A8, 1A9, and 1A10. *Int J Pharm* 2009;378:140–1.
- 33 Gupta RA, Sarraf P, Brockman JA, *et al.* Peroxisome proliferator-activated receptor gamma and transforming growth factor-beta pathways inhibit intestinal epithelial cell growth by regulating levels of TSC-22. *J Biol Chem* 2003;278:7431–8.
- 34 Yu T, Chen X, Zhang W, *et al.* Krüppel-Like factor 4 regulates intestinal epithelial cell morphology and polarity. *PLoS One* 2012;7:e32492.
- 35 Schweinfest CW, Spyropoulos DD, Henderson KW, *et al.* slc26a3 (dra)-deficient mice display chloride-losing diarrhea, enhanced colonic proliferation, and distinct up-regulation of ion transporters in the colon. *J Biol Chem* 2006;281:37962–71.
- 36 Nowarski R, Jackson R, Gagliani N, *et al.* Epithelial IL-18 equilibrium controls barrier function in colitis. *Cell* 2015;163:1444–56.
- 37 Farro G, Stakenborg M, Gomez-Pinilla PJ, *et al.* CCR2-dependent monocyte-derived macrophages resolve inflammation and restore gut motility in postoperative ileus. *Gut* 2017;66:2098–109.
- 38 Sheng YH, Hasnain SZ, Florin THJ, *et al.* Mucins in inflammatory bowel diseases and colorectal cancer. *J Gastroenterol Hepatol* 2012;27:28–38.
- 39 Dharmani P, Leung P, Chadee K. Tumor necrosis factor- α and MUC2 mucin play major roles in disease onset and progression in dextran sodium sulphate-induced colitis. *PLoS One* 2011;6:e25058.
- 40 Giessner C, Millet V, Mostert KJ, *et al.* Vnn1 pantetheinase limits the Warburg effect and sarcoma growth by rescuing mitochondrial activity. *Life Sci Alliance* 2018;1:e201800073.
- 41 Schmidt EK, Clavarino G, Ceppi M, *et al.* Sunset, a nonradioactive method to monitor protein synthesis. *Nat Methods* 2009;6:275–7.
- 42 Polansky O, Sekelova Z, Faldynova M, *et al.* Important metabolic pathways and biological processes expressed by chicken cecal microbiota. *Appl Environ Microbiol* 2015;82:1569–76.
- 43 Blacher E, Levy M, Tatirovsky E, *et al.* Microbiome-Modulated metabolites at the interface of host immunity. *J Immunol* 2017;198:572–80.
- 44 Liu H, Wang J, He T, *et al.* Butyrate: a double-edged sword for health? *Adv Nutr* 2018;9:21–9.
- 45 Tabuchi Y, Takasaki I, Doi T, *et al.* Genetic networks responsive to sodium butyrate in colonic epithelial cells. *FEBS Lett* 2006;580:3035–41.
- 46 Jin U-H, Cheng Y, Park H, *et al.* Short chain fatty acids enhance aryl hydrocarbon (Ah) responsiveness in mouse colonocytes and Caco-2 human colon cancer cells. *Sci Rep* 2017;7:10163.
- 47 Morgan XC, Tickle TL, Sokol H, *et al.* Dysfunction of the intestinal microbiome in inflammatory bowel disease and treatment. *Genome Biol* 2012;13:R79.
- 48 Scher JU, Sczesnak A, Longman RS, *et al.* Expansion of intestinal Prevotella copri correlates with enhanced susceptibility to arthritis. *Elife* 2013;2:e01202.
- 49 Perše M, Cerar A. Dextran sodium sulphate colitis mouse model: traps and tricks. *J Biomed Biotechnol* 2012;2012:718617:1–13.
- 50 Ueki I, Stipanuk MH. 3T3-L1 adipocytes and rat adipose tissue have a high capacity for taurine synthesis by the cysteine dioxygenase/cysteinesulfinate decarboxylase and cysteamine dioxygenase pathways. *J Nutr* 2009;139:207–14.
- 51 Levy M, Thaiss CA, Zeevi D, *et al.* Microbiota-Modulated metabolites shape the intestinal microenvironment by regulating NLRP6 inflammasome signaling. *Cell* 2015;163:1428–43.
- 52 Seregin SS, Golovchenko N, Schaf B, *et al.* NLRP6 Protects Il10^{-/-} Mice from Colitis by Limiting Colonization of Akkermansia muciniphila. *Cell Rep* 2017;19:733–45.
- 53 Kang M, Qin W, Buya M, *et al.* VNN1, a potential biomarker for pancreatic cancer-associated new-onset diabetes, aggravates paraneoplastic islet dysfunction by increasing oxidative stress. *Cancer Lett* 2016;373:241–50.
- 54 Washino S, Hosohata K, Oshima M, *et al.* A novel biomarker for acute kidney injury, Vanin-1, for obstructive nephropathy: a prospective cohort pilot study. *Int J Mol Sci* 2019;20. doi:10.3390/ijms20040899. [Epub ahead of print: 19 Feb 2019].
- 55 Zhu X, Cooper RS. Admixture mapping provides evidence of association of the VNN1 gene with hypertension. *PLoS One* 2007;2:e1244.
- 56 Santoru ML, Piras C, Murgia A, *et al.* Cross sectional evaluation of the gut-microbiome metabolome axis in an Italian cohort of IBD patients. *Sci Rep* 2017;7:9523.
- 57 Lloyd-Price J, Arze C, Ananthakrishnan AN, *et al.* Multi-Omics of the gut microbial ecosystem in inflammatory bowel diseases. *Nature* 2019;569:655–62.
- 58 Bell CJ, Gall DG, Wallace JL. Disruption of colonic electrolyte transport in experimental colitis. *Am J Physiol* 1995;268:G622–30.



SUPPLEMENTARY DATA Fig.S1

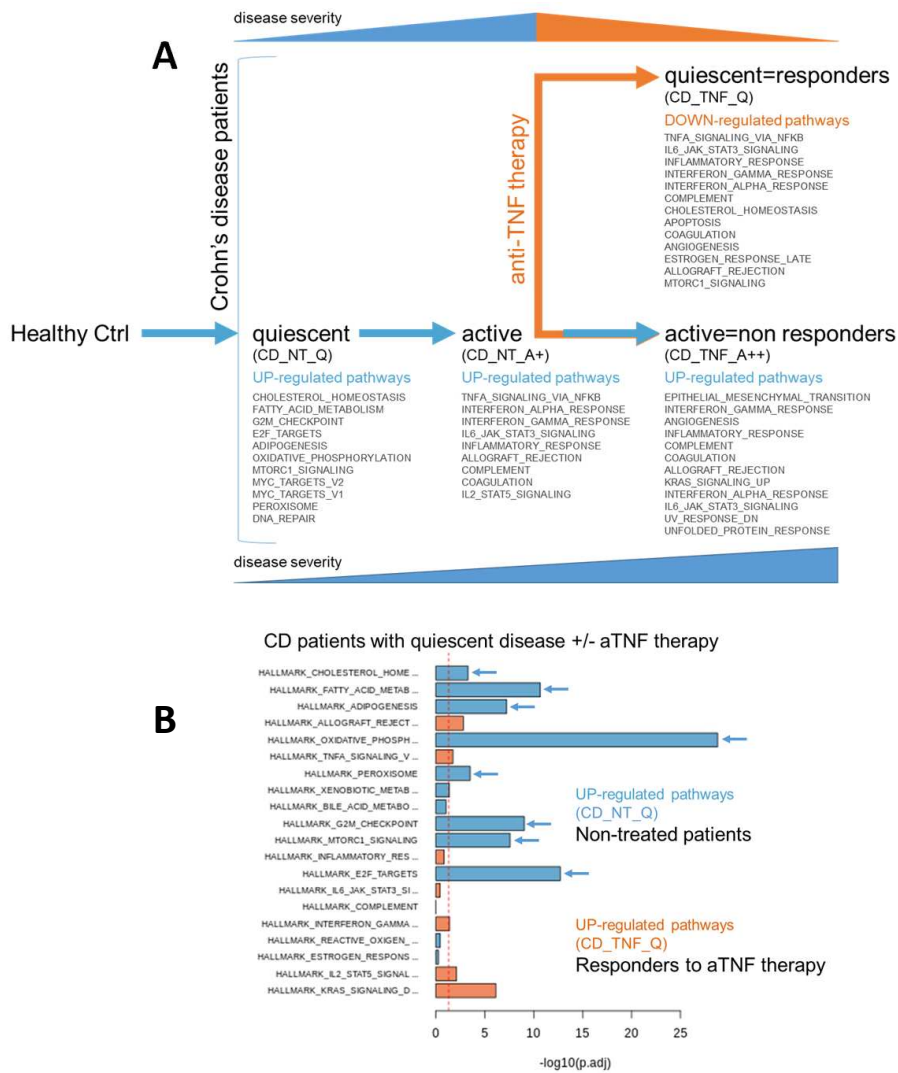
VNN1 expression in human colon observed in IBD biobanks.

(A). **VNN1 is poorly expressed in healthy colon but its expression is induced in colonocytes and goblet cells in inflamed UC colons.** Upper panel: t-SNE plot showing the heterogeneity of human colonic epithelial cells (n = 3; CT, crypt top) Lower panels: distribution of VNN1 expression in the different cell populations under inflammatory and non-inflammatory conditions. Data were extracted from [Parikh K et al., Data from: colonic single epithelial cell census reveals goblet cell drivers of barrier breakdown in inflammatory bowel disease gene expression Omnibus Repository (GSE116222), 2019. Available: <https://www.ncbi.nlm.nih.gov/geo/query/acc.cgi?acc=GSE116222>].

(B). **Description of the IBD biobank.** The IBD biobank was generated starting with biopsy samples collected from patients suffering from CD or UC and diagnosed as clinically quiescent (Q) or in active phase of the disease (A) with various degrees. The severity of the disease is graduated by “+”. Patients were either not-treated at the period of diagnosis (NT) or under various therapies such as 5-ASA, anti-TNFalpha biologics (aTNF) or immunosuppressors (IS). Controls were taken from non-inflammatory healthy portions of colon (CTRL).

(C). **Description of the clinical scoring of the IBD patients from the biobank.** The scoring of the IBD severity was determined by physician global assessment (PGA) as described (upper table). Disease activity was further measured by endoscopy using the MAYO endoscopic subscore (MES) for UC patients (lower table). CD patients were stratified into 2 categories following the STRIDE consensus (L. Peyrin-Biroulet et al Am Journal of gastroenterology 2015, STRIDE II D. Turner et al, gastroenterology 2021), whether they were in remission with endoscopic healing and without ulcerations (SES-CD ≤2 points) or had active disease with ulcers.

(D). **VNN1 expression in UC and CD patients according to the PGA and endoscopic scores.**



SUPPLEMENTARY DATA Fig.S2

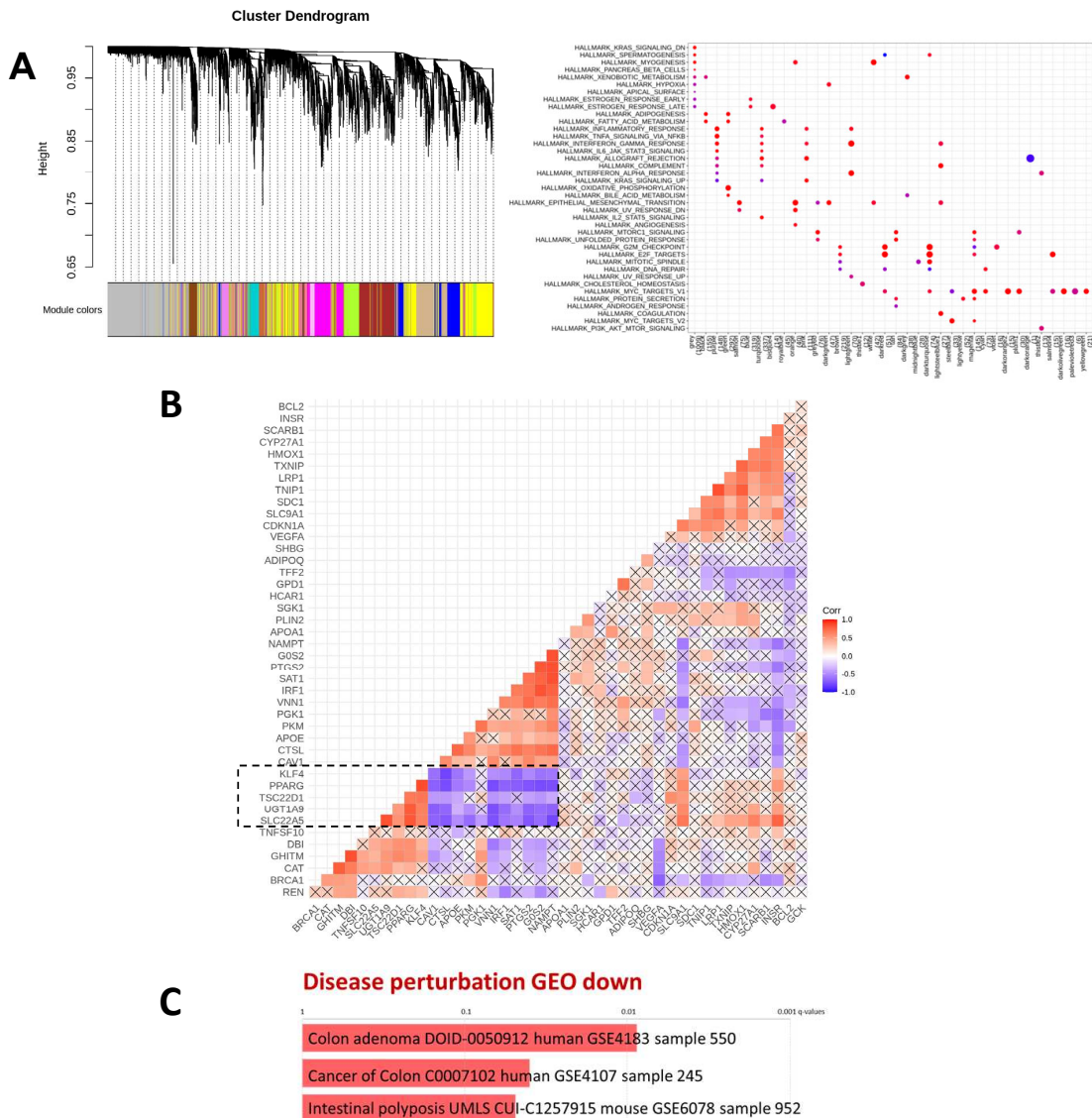
Transcriptomic analysis of human colonic RNA sequencing profiles from control and patients enrolled in a stratified IBD biobank.

(A) Evolution of the transcriptomic profiles of the colon samples according to gradation of Crohn's disease and responsiveness to anti-TNF alpha biologics.

Systematic comparison of all samples with each other using an EGSEA approach documenting the evolution of transcriptional signatures at different stages of the disease. CD patients with clinically resting disease (CD_NT_Q) already show detectable transcriptional changes when compared to healthy controls, featuring enhanced energy/metabolic signatures (fatty acid metabolism, oxidative phosphorylation; MTORC1 signaling...), and repair/proliferation signatures (DNA repair, MYC-targets, E2F-targets; G2M-checkpoint...). These modifications reflect the presence of compensatory mechanisms to cope with a subclinical mucosal stress. As anticipated, CD patients with active disease (CD_NT_A+) display a dominant cytokine-driven (TNF, IFN, IL-6 mostly) inflammatory signature that is totally down-regulated in anti-TNF responders (CD_TNF_Q).

Failure of anti-TNF biologics in non-responder patients (CD_TNF_A++) with aggravated disease is accompanied by a reinforced inflammatory pattern and signs of a strong tissue disorganization, showing enhanced markers of epithelial-to-mesenchymal transition (EMT), angiogenesis and unfolded protein response (UPR).

(B) Comparison of transcriptomic profiles between a clinically quiescent state for patients developing moderate disease and a state that became quiescent in responder patients to anti-TNF therapy. The anti-TNF responders (CD_TNF_Q) does not show the metabolic/repair profile observed in non-treated patients with a resting disease (CD_NT_Q) when compared to healthy controls (blue arrows)(Fig.1C). This suggests that the attenuation of inflammation by anti-TNF biologics helps tissue recovery.



SUPPLEMENTARY DATA Fig.S3

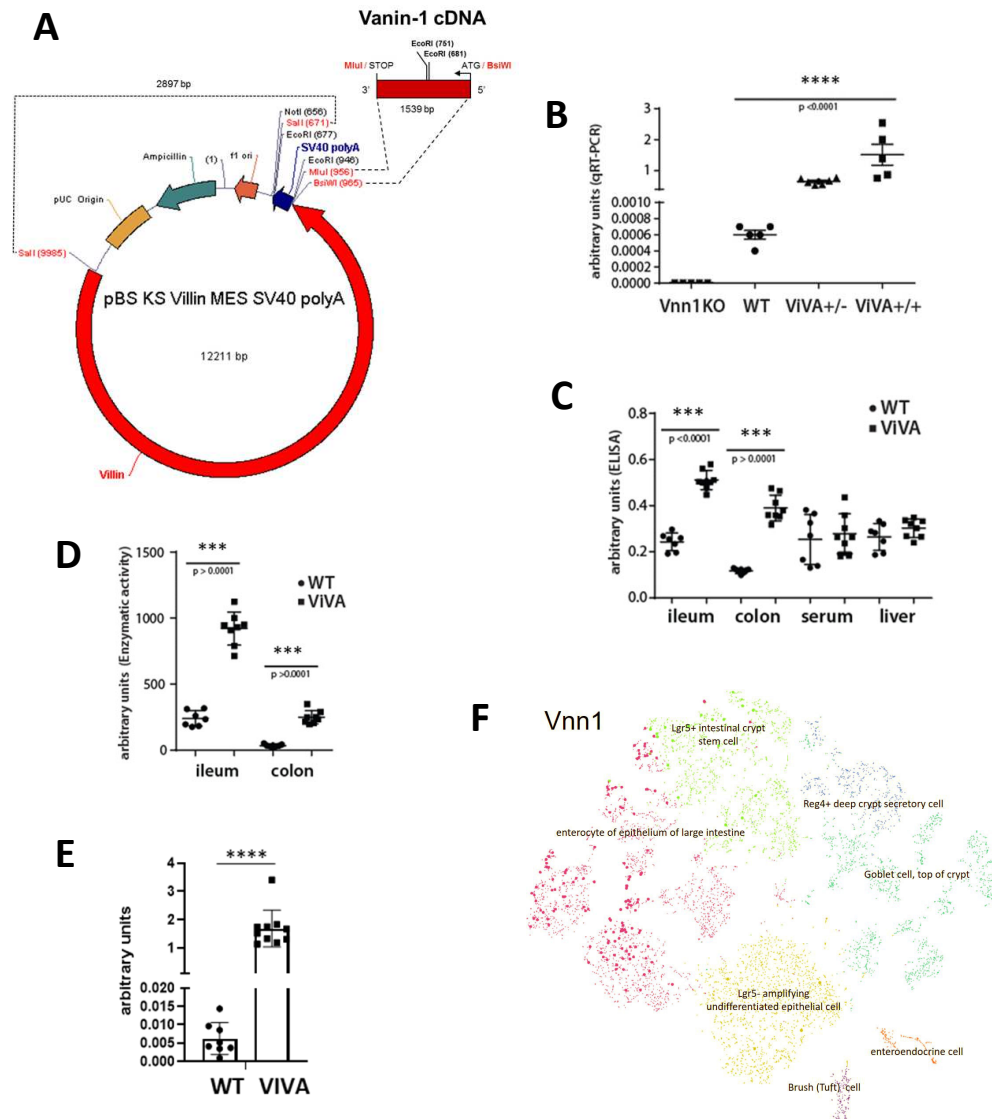
Exploration of PPARgamma co-expression modules in IBD.

(A) Identification and functional exploration of expression modules in IBD.

We applied the WGCNA (weighted gene co-expression network analysis) clustering method to produce the co-expression network from the RNA-Seq data. The left panel represents a dendrogram of the resulting clustering that describes all the modules of coexpressed genes generated. Among these a VNN1-type module ("purple") and a module linked to PPARgamma expression ("black"). In the right panel, all gene modules were examined using KEGG pathway analysis.

(B-C) Partial shut down of a PPARgamma program in severe diseases.

PPARgamma was found to be under-expressed in acute IBD. Therefore, we tested the expression of a list of already described PPARgamma target genes in human in our IBD samples [Fang L. et al., Data from : PPARgene: a database of experimentally verified and computationally predicted PPAR target genes PPAR research 6042162, 2016. Available: PPARgene database - Downloads [Accessed 12 Jan 2016].]. (B) Correlation showing that not all PPARgamma target genes follow PPARgamma expression in IBD (including Vnn1). However, a small group does (dotted box). Crossed comparisons exhibit p-value higher than 0.05. (C) Similarly, this small gene set was found to be also shut down in others colon pathologies (Enrichr analysis).



SUPPLEMENTARY DATA Fig.S4

VIVA transgenic mice specifically overexpress an active Vnn1 pantetheinase in gut epithelium.

(A) Transgene DNA construct used for the generation of the VIVA mouse. The Vnn1 gene is under control of the Villin promoter. Villin is expressed in all intestinal epithelial cells though the expression is higher in villus cells than crypt cells (El Marjou et al., 2004).

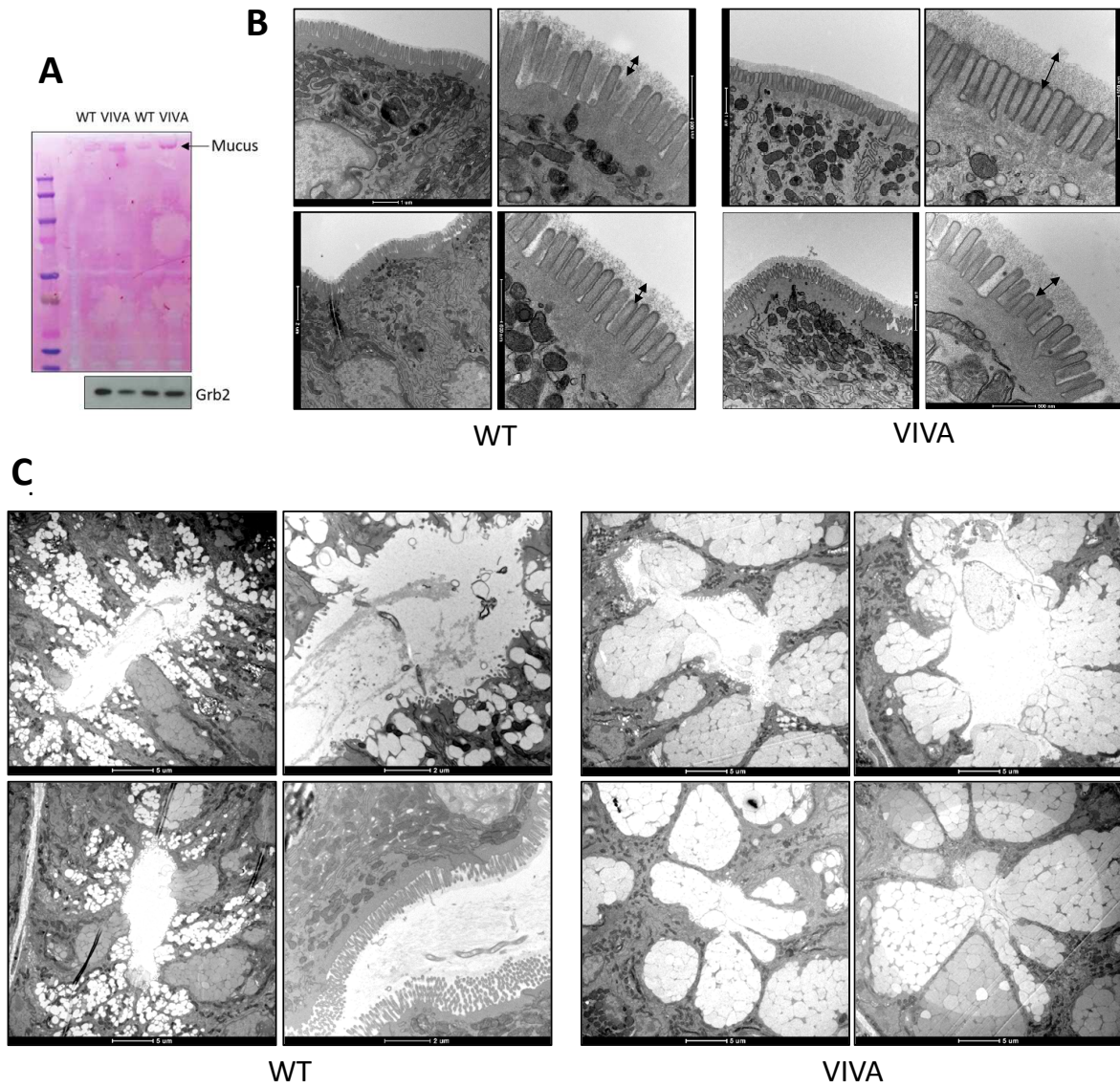
(B) Enhanced Vnn1 transcript expression in colon of VIVA mice (qRT-PCR).

(C) Specific enhanced Vnn1 protein expression in VIVA gut tissues (specific Vnn1 ELISA).

(D) Enhanced Vnn1 pantetheinase activity in VIVA gut tissues (specific enzymatic assay).

(E) Enhanced Vnn1 transcript expression in isolated colonocytes from VIVA mice (qRT-PCR).

(F) Single cell sequencing data that confirmed that Vnn1 is mostly expressed by colonocytes (enterocytes of epithelium of large intestine) at steady state in WT animals. Data were extracted from [Tabula Muris Consortium. Data from: transcriptomic characterization of 20 organs and tissues from Mus musculus at single cell resolution. Gene expression Omnibus Repository (GSE109774). Available: <https://www.ncbi.nlm.nih.gov/geo/query/acc.cgi?acc=GSE109774> [Accessed 19 Mar 2018].].



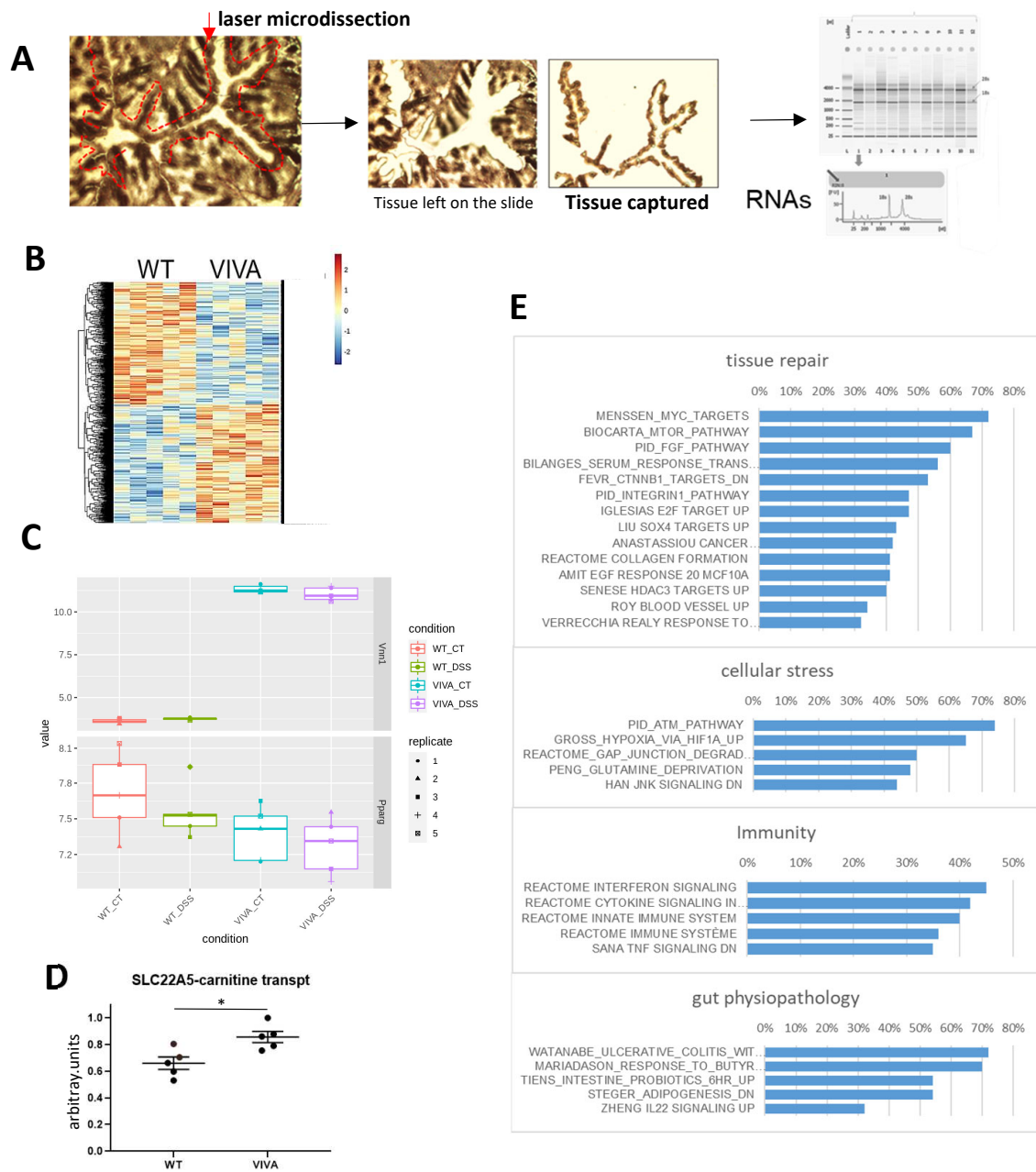
SUPPLEMENTARY DATA Fig.S5

Improved barrier function and crypt protection in VIVA colons

(A) Enhanced mucus detection by PAS-coloured membrane blot

(B) Electron microscopy study showing accumulation of mucus deposition at the surface of the VIVA colon mucosa.

(C) Reduced mucin depletion and bacterial invasion in crypts from DSS treated VIVA mice



SUPPLEMENTARY DATA Fig.S6

Transcriptomic analysis of the microdissected mucosa of VIVA mice.

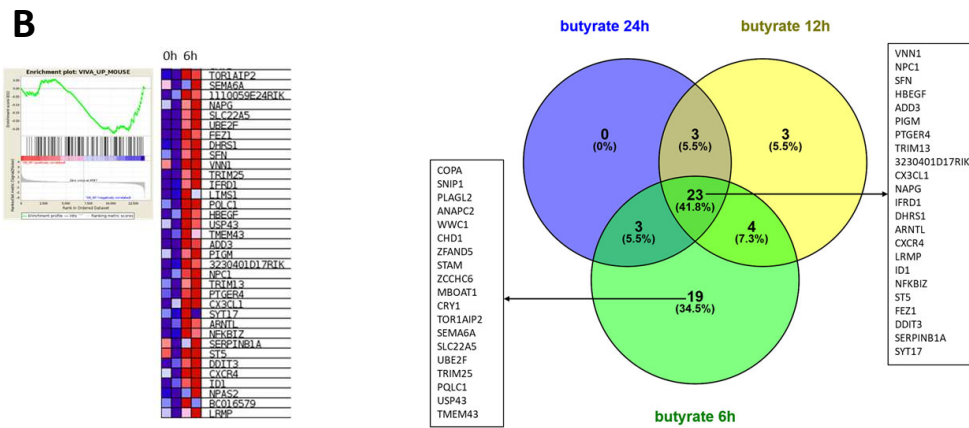
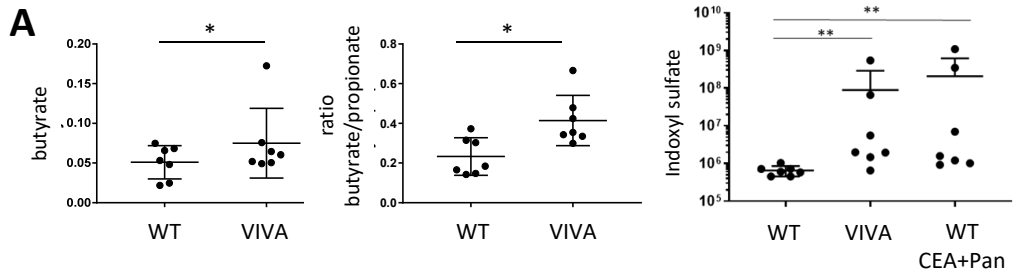
(A) Description of the Laser micro-capture of the colonocyte layer for a transcriptomic study.

(B) Heatmap display of a transcriptomic analysis of microdissected mucosa (n=5) representing the differentially expressed genes between WT and VIVA colonocytes at steady state. The relative expression levels ranked from high (red) to low (blue).

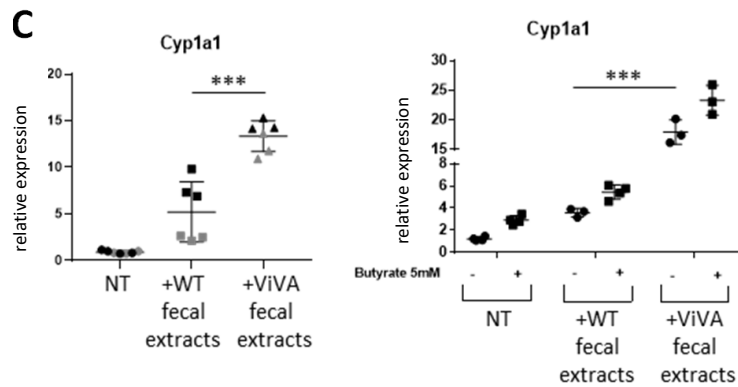
(C) Comparative expression of Vnn1 and PPARgamma in colons of WT and VIVA mice in control (CT) or colitis (DSS) conditions.

(D) Enhanced expression of the carnitine transporter SLC22A5 in isolated colonocytes from VIVA mice (qRT-PCR).

(E) A colonocyte transcriptomic signature evocative of epithelial crisis in response to stress and damage during the early phase of colitis (WT_DSS_UP)(GSEA analysis).



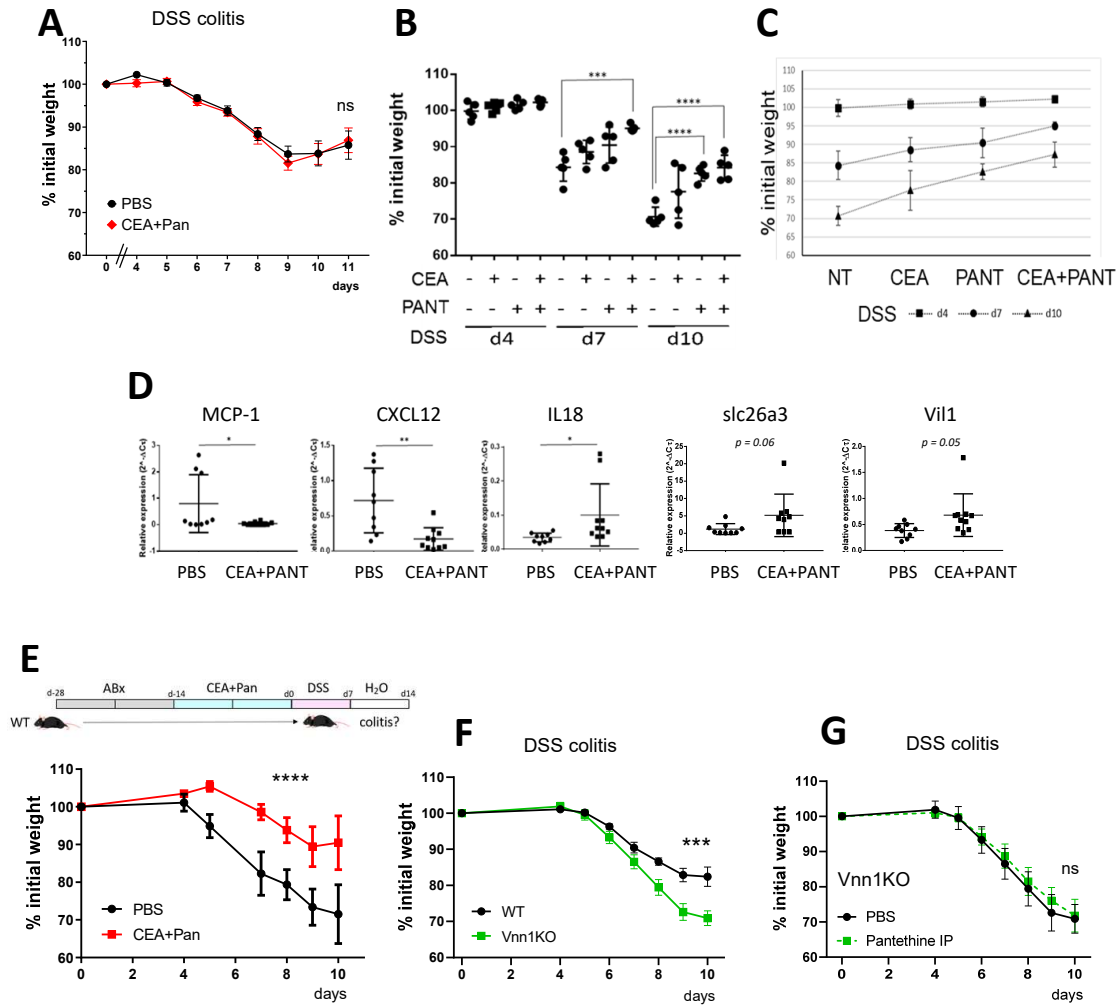
GSE4410: Genes responsive to sodium butyrate in colonic epithelial cells.
 MCE301 mouse colonic epithelial cells exposed to 2mM sodium butyrate ;
 Time course : 0h – 6h -12h – 24h



SUPPLEMENTARY DATA Fig.S7

Enrichment in butyrate and and indoxyl sulfate in feces from VIVA mice.

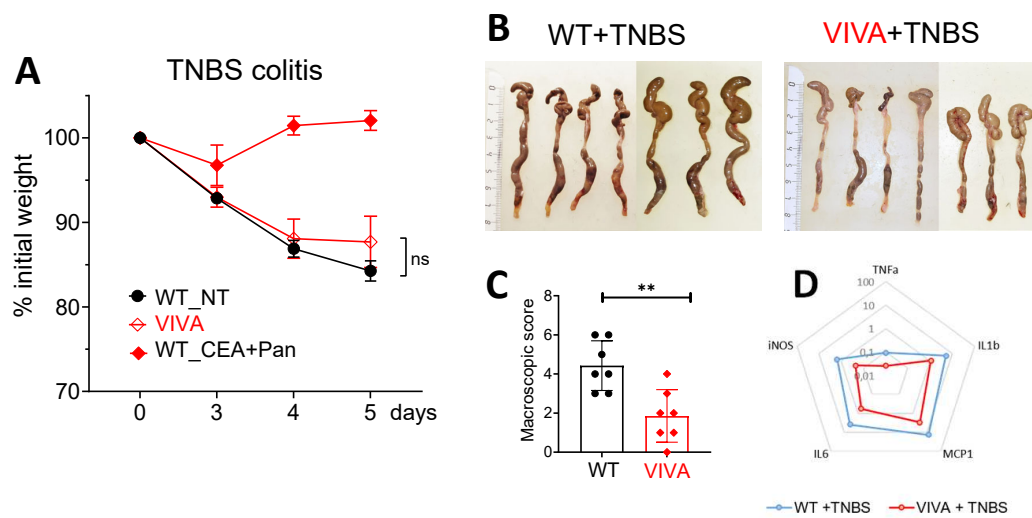
(A) Augmented levels of butyrate (NMR analysis) and Indoxyl sulfate (LC-MS analysis) in feces from VIVA mice .
 (B) Butyrate responsive genes up-regulated in VIVA colonocytes (GSEA analysis). Data were extracted from Tabuchi Y et al., Identification of genes responsive to sodium butyrate in colonic epithelial cells. *Biochem Biophys Res Commun* 2002;293:1287–94 [https://www.ncbi.nlm.nih.gov/geo/query/acc.cgi?acc=GSE4410.1016/S0006-291X\(02\)00365-0](https://www.ncbi.nlm.nih.gov/geo/query/acc.cgi?acc=GSE4410.1016/S0006-291X(02)00365-0)
<http://www.ncbi.nlm.nih.gov/pubmed/12054516>
 (C) VIVA fecal extracts stimulate the expression of the butyrate-responsive marker CYP1A1 in Caco2 cells.



SUPPLEMENTARY DATA Fig.S8

Preconditioning with Cysteamine + Pantothenate protects WT mice from severe DSS-colitis.

- (A) CEA+Pan therapy during the course of colitis has no effect on the development of the disease.
 (B-C) Respective effect of the single or combined administration of Cysteamine and Pantothenate.
 (D) A gene signature indicative of healthy mucosa.
 (E) CEA+PANT treatment affects the resilience of the microbiota.
 (F) Vnn1-deficient mice (Vnn1KO) develop a severe DSS colitis compared to WT controls.
 (G) Administration of pantethine has no beneficial effect on Vnn1KO mice exposed to DSS.



SUPPLEMENTARY DATA Fig.S9

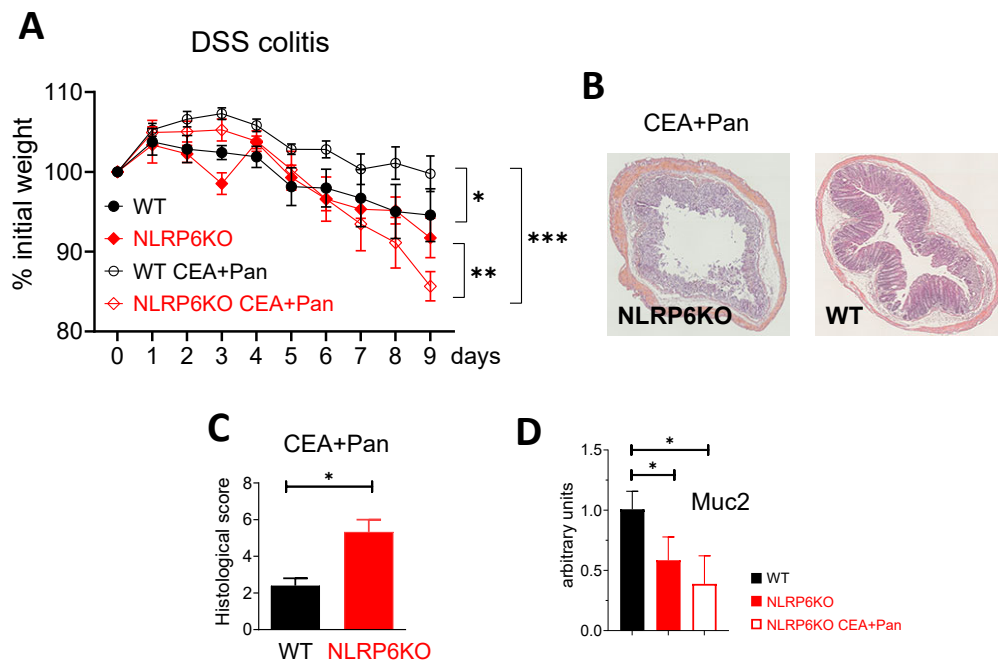
Cysteamine + Pantothenate therapy reduce TNBS colitis in VIVA mice.

(A) Comparative mouse weight loss in the early phase of TNBS-induced experimental colitis in control WT non-treated (WT_NT) versus VIVA mice, and WT submitted to cysteamine + pantothenate administration (WT_CEA+Pan).

(B) Representative images of the extracted colons from WT and VIVA mice at day 5 of the TNBS protocol showing a better preserved morphology of VIVA colons that of control mice.

(C) Macroscopic score between WT and VIVA colons according to the TNBS scoring as described in table.

(D) Radar diagram representation of RT-PCR results quantifying cytokine/enzyme transcripts associated with acute inflammation in VIVA colons.



SUPPLEMENTARY DATA Fig.S10

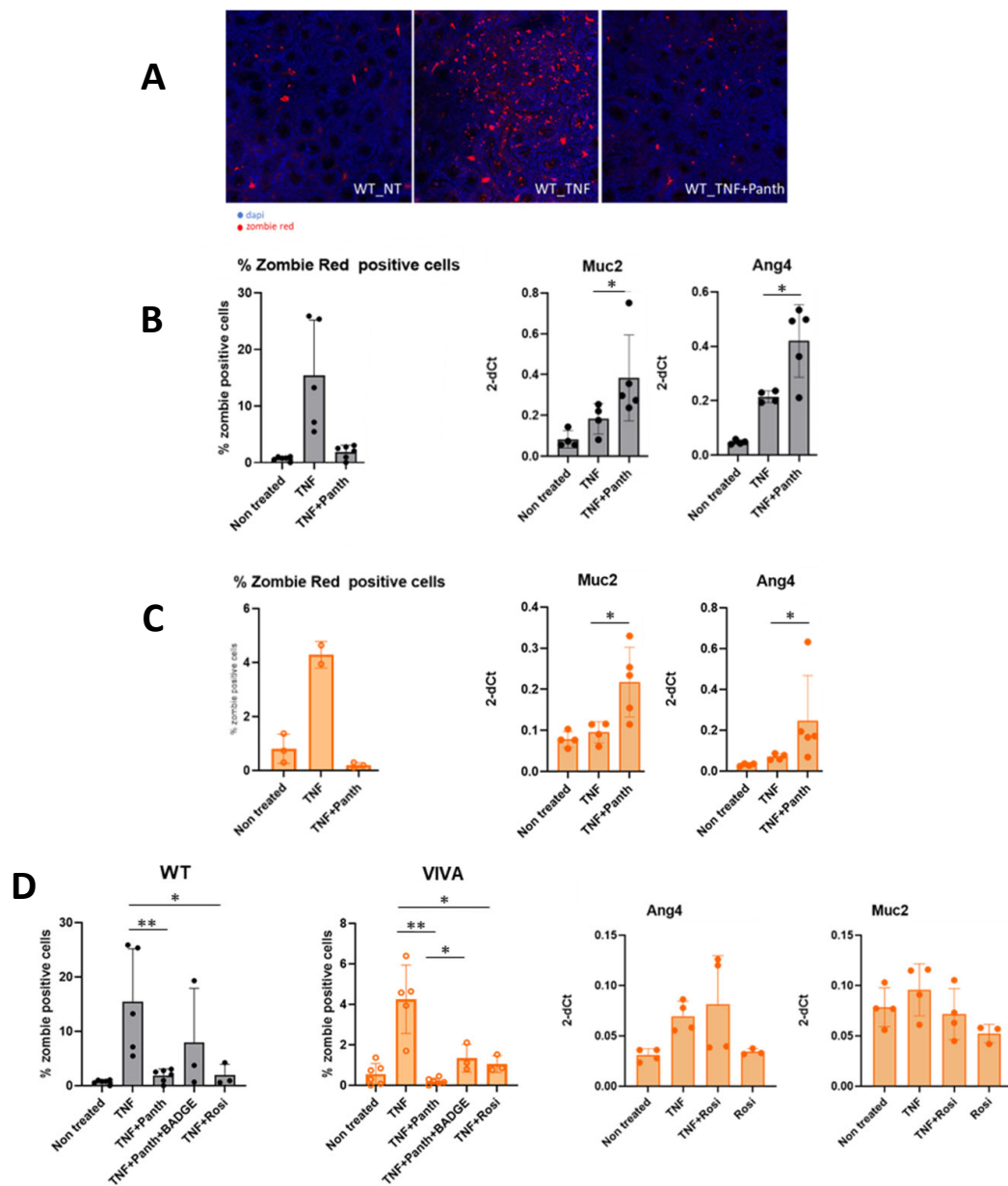
Cysteamine + Pantothenate therapy reduce TNBS colitis in VIVA mice but not DSS colitis in NLRP6-deficient mice

(A) Monitoring of the total body weight loss in pre-treated (CEA+Pan) or non-treated WT or NLRP6-deficient mice (NLRP6KO) during DSS-colitis.

(B) Representative Hematoxylin-Eosin staining of paraffin-embedded sections prepared from colons of CEA+Pan-treated WT and NLRP6KO mice.

(C) Anatomopathological scoring of colitis severity between CEA+Pan-treated WT and NLRP6KO mice based on colon sections examination.

(D) RT-PCR quantification of Muc2 expression in whole colons of WT and CEA+Pan-treated or not NLRP6KO mice.



SUPPLEMENTARY DATA Fig.S11

Pantethine supply promotes epithelial restoration of WT and VIVA organoids post TNF α -induced cell death.

2D organoid cultures in Air-Liquid Interface (ALI) were prepared as described (Wang, Chiang et al. 2019). WT or VIVA colon organoids were exposed to TNF α (30ng/ml) for 3 days (TNF) and treated (TNF+Panth) or not with pantethine (500 μ M) during the whole experiment. Epithelial restoration was followed 2 days after TNF α withdrawal.

(A) Representative immunofluorescence staining of cell death in WT colon organoids exposed to the various conditions as indicated using the zombie red dye.

Quantification in WT (B) or VIVA (C) colon organoids of the cell death (% of Zombie Red positive cells) and the expression by RT-PCR of the transcripts encoding for the epithelial products Muc2 (mucus) and Ang4 (anti-microbial peptide).

(D) To study the role of PPAR γ in these processes, we treated WT or VIVA organoids exposed to TNF α with the PPAR γ agonist rosiglitazone (1 μ M)(TNF+Rosi). To investigate whether PPAR γ interfere with or participate to the Vnn1-pantetheinase beneficial environment we added the PPAR γ antagonist BADGE (1 μ M) during the pantethine treatment (TNF+Panth+BADGE). In each condition, cell death was examined by Zombie Red staining and Muc2 and Ang4 expression was assessed by RT-PCR.

**% of ulceration: morphometric assessment
(ulcerative foci/total length of mucosa per swiss roll)**

- 0 - 0%
- 1 - 1 - 10%
- 2 - 11 - 20 %
- 3 - 21-50%
- 4 - 51-100%

Inflammation severity:

- 0 - none
- 1 - minimal
- 2 - moderate
(some inflammatory foci, sometimes disrupting glandular architecture)
- 3 - marked
(abundant inflammatory population, disrupting glandular architecture).

Inflammation extend:

- 0 - none
- 1 - mucosa
- 2 - mucosa and submucosa
- 3 - transmural

Crypt damage:

- 0 - none
- 1 - 1/3 crypt damaged
- 2 - 2/3 crypt damaged
- 3 - crypt loss, epithelium intact
- 4 - crypt loss, epithelium loss

Table S1: Criteria of scoring for histological assessment of colitis severity.

	Forward primer sequence	Reverse primer sequence
Actin	TGGAATCCTGTGGCATCCATGAAACC	TAAAACGCAGCTCAGTAACAGTCCG
Villin	TCAAAGGCTCTCTCAACATCAC	AGCAGTCACCATCGAAGAAGC
Spdef	AAGGCAGCATCAGGAGCAATG	CTGTCAATGACGGGACACTG
Ang4	GGTTGTGATTCTCCAACCTCTG	CTGAAGTTTTCTCCATAAGGGCT
Retnlb	AAGCCTACACTGTGTTTCCTTTT	GCTTCCTTGATCCTTTGATCCAC
slc22a5	ACTGTGCCAGGGGTGCTAT	GCAACTGAGGCTTCGTAGAAT
Slc26a3	TTTCCAGATCAGGGGTTTCAG	CAGCAAACGCATCAGCATT
Mcp1	CTCACCTGCTGCTACTCATT	GCTTGAGGTGGTTGTGAAAA
Cxcl12	TGCATCAGTGACGGTAAACCA	TTCTTCAGCCGTGCAACAATC
Itln1	CAGCACTTGGGACATAATCTGT	TCCTTCTCCGTATTTCACTGGG
Il18	GACAGCCTGTGTTTCGAGGA	TGGATCCATTTCTCAAAGG
Vnn1	TGTGCGTTTCACCAGGGAT	ACTTGAGGGTCTGGGATCTCC
Muc2	ATGCCACCTCCTCAAAGAC	GTAGTTTCCGTTGGAACAGTGAA
Muc4	CCTCCTCTTGCTACCTGATGC	GGAACCTGGAGTATCCCTTGTG
human ACTIN	CGACAGGATGCAGAAGGAGA	CGCTCAGGAGGAGCAATG
human CYP1A1	GACCACAACCACCAAGAAC	AGCGAAGAATAGGGATGAAG

Table S2: Sequences of primers used for PCR experiments.

SUPPLEMENTARY METHODS

IBD biobank and RNAseq studies.

Biopsies samples from IBD patients were collected at the department of gastroenterology (Pr. Grimaud, APHM HOPITAL NORD, Marseille), and registered under ClinicalTrials.gov Identifier: NCT02304666. RNA was extracted from colonic biopsies using the Qiagen AllPrep RNA/DNA Mini Kit. RNA integrity was measured by AGILENT bioanalyzer. RNAseq was carried out at the platform GenomEast IGBMC, ILLKRICH, France. All samples were sequenced in 50-length Single-Read. Reads were mapped onto the hg38 assembly of the Homo sapiens genome using Tophat 2.0.14 and bowtie version 2-2.1.0. Only uniquely mapped reads have been retained for further analyses. Quantification of gene expression has been performed using HTSeq-0.6.1 with annotations coming from Ensembl 87. Read counts have been normalized across libraries with the median-of-ratios method proposed by Anders and Huber. To check normalization, Relative Log Expression (RLE) plots were drawn. Genes with less than 10 counts in the sum of all samples were discarded for further analyses. Counts were scaled by trimmed mean of M-values (<https://doi.org/10.1093/bioinformatics/btp616>) for EGSEA (<https://doi.org/10.1093/bioinformatics/btw623>), or normalized by the pseudolog2 of the variance-stabilizing transformation (<https://doi.org/10.1186/s13059-014-0550-8>) for WGCNA (<https://doi.org/10.1186/1471-2105-9-559>), accordingly to their respective guidelines.

EGSEA was computed against all built-in ontologies using eight methods: camera, safe, gage, padog, zscore, gsva, globaltest and ora. Results were sorted by the average rank of the methods. WGCNA was computed using unsigned network with biweight midcorrelation and softPower=13. Each module was further 2-means clustered to separate correlated and anti-correlated patterns, and their genesets were queried for functional enrichment against MSigDB Hallmark (<https://dx.doi.org/10.1016%2Fj.cels.2015.12.004>) using clusterProfiler (<https://doi.org/10.1089/omi.2011.0118>).

VIVA mouse generation.

The pBluescript II KS Villin MES SV40 polyA plasmid containing 9kb of the murine Villin regulatory regions and a multiple cloning region (MCS) at its 3' side was kindly provided by Dr. Sylvie Robine (UMR144, Institut Curie, Paris). 1539bp of the Vnn1 complete cDNA coding sequences were inserted into the MCS using the MluI-BsIWI restriction sites (suppl.data). The linearized 10853bp Sall-digested Villin-Vnn1 transgene was purified using the Qiaquick gel extraction kit (Qiagen). The transgene was then injected in fertilized oocytes pronuclei from

C57BL/6xCBA/j hybrid mice. Transgene transmission to germinal cells was verified by a PCR strategy using primers encompassing the 793bp long intron 3-4 segment. Afterward mice were backcrossed for 9 generations on the C57BL/6 background. Expression of the transgene in mouse organs was monitored by qRT-PCR and ELISA, and pantetheinase activity in tissue was measured.

Laser Capture Microdissection (LCM) and transcriptomic analysis.

A 1cm segment of the distal colon was recovered from 4-day DSS-treated mice and frozen embedded in Tissue-Tek OCT (Sakura-Finetek Europe). The epithelial cell layer was captured on HE stained colon sections (5 μ m) using the ArcturusXT Laser Capture Microdissection (LCM) System (Applied Biosystems) following manufacturer's procedures. Total RNA was extracted using the Arcturus PicoPure RNA Isolation kit (Applied Biosystems). RNAs samples validated on Agilent 2001 bioanalyzer (Agilent Technologies) were used for hybridization on Affymetrix genchip mouse genome arrays (platform GenomEast IGBMC, ILLKRICH, France). Analysis of data was performed by the Bioinformatic platform at CIML. The mouse Gene 1.0 ST CEL files corresponding to WT (n=5) and VIVA (n=5) mice treated or not with DSS, were pre-processed through Bioconductor in the R statistical environment (version 3.2.2). Quality control of the array hybridization (NUSE and RLE plot) and normalization of the raw Affymetrix expression data with Robust Multi-array Average (Irizarry et al.2003, Biostatistics) were performed using the oligo package. Differentially expressed genes (DEG) between DSS-treated and control mice were selected for a FDR (Benjamini-Hochberg correction) <0.05 after empirical Bayes processing using the Limma package. DEGs were used as genesets for BubbleMap analysis where each bubble is a GSEA result and summarizes the information from the corresponding enrichment plot. GSEA allowed the extraction of the leading edges for each set of DEGs between two experimental conditions. Selected genes were submitted to Enrichr software.

Gene expression.

Total mRNA from tissues or cells was purified using the RNeasy Mini Kit (Qiagen). For qRT-PCR analysis, 0.5–1 μ g RNA was reverse transcribed with the SuperScript II RT kit (Life Technologies). Amplification was performed on a 7500 Fast Real Time PCR system (Applied Biosystems) using SYBR green Master Mix (Takara) and specific primer pairs (Table S2). Expression levels were normalized to the control gene actin. To assess AMP gene expression

in isolated colonocytes, samples were normalized using the expression of the SPDEF gene as a marker of goblet cell enrichment.

Flow cytometry.

Mice were sacrificed at day 4 of the DSS treatment and colons were washed with ice cold PBS, cut into small pieces, washed again with EDTA-HBSS several times, and digested with Collagenase VIII from *Clostridium histolyticum* (Sigma-Aldrich) to obtain single cell suspensions. Cells were recovered using a Percoll gradient and stained with specific antibodies: Cd11b (M1/7); CD64 (X54-5/7.1); CD3 (17A2); NK1.1 (PK136); CD19 (6D5); Ly6G (1A8); Ly6C (Al-21); CD45 (104); CD24; CD11c (N418) and SYTOX Green Nucleic Acid Stain (Thermo Fisher Scientific). Cytometry analysis was performed on a LSR II flow cytometer and data analyzed with the FACSDIVA software (BD Biosciences). Lamina propria CD64⁺ gut monocytes were gated in CD11b⁺ CD24⁻ CD45⁺ Lin⁻ and Ly6G⁺ neutrophils in CD45⁺CD11b⁺ CD11c⁺ CD45⁺ live cells, respectively.

Epithelial permeability.

Fluorescein isothiocyanate–dextran (Sigma-Aldrich) was administered to mice at 44mg/100g body weight by oral gavage. 5 hours after gavage, blood was recovered by retro orbital puncture from anesthetized mice (3% isoflurane). Plasma FITC fluorescence was measured using a TECAN Infinite M 1000 PRO microplate reader.

Electron microscopy analysis.

Samples were prepared using the NCMIR protocol for serial blockface scanning electron microscopy (West et al, 2010). 70-nm ultrathin sections were performed on a Leica UCT Ultramicrotome (Leica) and deposited on formvar-coated slot grids. The grids were observed in an FEI Tecnai G2 at 200 KeV, and acquisition was performed on a Veleta camera (Olympus). The size of the apical mucus layer was measured on 17 images per mouse and 3 mice per genotype. Mucus accumulation and crypt-invading bacteria were scored as indicated in fig. 3I in 3 different mice per genotype.

Preparation of isolated mice colonocytes.

Colons, from the caecum to the rectal ampulla, were rapidly removed and flushed with calcium free HBSS, then everted, ligated at the proximal and distal ends, and placed in 10ml of HBSS-0.25%BSA 5mM EDTA. After an incubation for 30 minutes at 37°C in a shaker, they were

rinsed in fresh calcium-free HBSS and placed again in 10ml of HBSS-0.25% BSA. Vigorous manual stirring for 2 minutes readily disaggregated colonocytes, then separated by centrifugation (500g, 2 min, 4°C). The cells were washed twice in PBS and used for IF (Mitoxox), lactate quantification, or qRT-PCR.

Cell culture.

Human colon Caco-2 cells were maintained in DMEM 10% FBS, 1% sodium pyruvate, 1% non-essential amino acids and 1% penicillin-streptomycin. To induce differentiation and polarization, cells were grown in 24-well plate with permeable PET membrane filter supports (Transwell 0.4µM pore size). Culture medium was changed 3 times a week and experiments were conducted on days 17-21 post-seeding. Fecal filtrates were added in the apical medium. Caco-2 cell extracts were collected after 16hr for qRT-PCR.

Fecal extracts preparation.

100mg of mice feces were homogenized in 1ml of Phosphate buffer saline containing 50µg/ml gentamycin, 100Units/ml penicillin and 100µg/ml streptomycin. The homogenate was centrifuged (10000rpm, 15min, 4°C) and the supernatant filtrated on a Nanosep column with 3K Omega (Pall). The eluate was immediately used to treat the cells.

Measure of urinary concentrations of indoxyl sulfate.

Human urines were collected through the I-BANK IBD cohort generated at the Department of gastroenterology University Hospital of Nancy (Pr. L. Peyrin-Biroulet). Indoxyl sulfate was measured in urine of mice and human using the Indicant Assay kit (Sigma). Data processing was done by establishing a calibration curve.

Monitoring of Vnn1 protein and pantetheinase activity.

The mouse Vnn1 ELISA and quantification of pantetheinase activity were done as described (Rommelaere, S et al, 2013).

Sunset analysis for in vivo quantification of protein translation

30 min after ip injection of 40nmol/g of puromycin (Sigma-Aldrich), colons were flushed in PBS, and frozen in liquid nitrogen for western blots (WB) or snap frozen in Tissue-Tek OCT (Sakura-Finetek Europe) for IF analysis. Cryosections were fixed / permeabilized for 30min (Kit from BD biosciences), incubated 1h30 at RT with the AF488 anti-puromycin antibody

(Millipore) diluted in Perm/Wash Buffer, and counterstained with DAPI. For WB, frozen tissues were homogenized 20 sec in ice-cold RIPA buffer (25mM Tris pH 7.6, 150mM NaCl, 1% NP40, 1% DOC, 0.1%SDS, protease inhibitors). After centrifugation (10000 rpm, 10min, 4°C), 50µg of proteins were subjected to 10% SDS-PAGE, and transferred onto a PVDF membrane. To verify loading, blots were stained with Ponceau S. Membranes were saturated with PBS-5% BSA- 0.5% Tween for 1h followed by an overnight incubation at 4°C with a mouse IgG2a monoclonal anti-puromycin antibody (Millipore) in PBS 5% BSA. After 15 min wash in PBST, they were incubated for 1h at RT in 5% BSA-PBS containing horseradish peroxidase-conjugated anti-mouse IgG Fc antibody (Sigma-Aldrich). After 15 min wash, blots were developed with enhanced chemiluminescence (ECL) reagent (Pierce,ThermoFisherScientific, Rockford, IL, USA). Densitometric measurements were performed with ImageJ (NCBI).

MitoSox/MitoTracker

Colonocytes were seeded in Chambered Coverglass (Lab-Tek Nunc) coated with Cell-Tak (Corning), and filled with HBSS/Ca/Mg containing 50nM MitoTracker Green FM reagent plus 1µM MitoSox Red, a mitochondrial superoxide indicator (Invitrogen). After 15min of incubation at 37°C, the cells were washed in warm buffer, then observed with a confocal microscope.

Caco-2 cells were seeded in Lab-Tek in a volume of 0.4ml and stimulated with 40µl of filtrated fecal extracts, 20µM Antimycin A (Sigma-Aldrich) or 1mM sodium butyrate. 24hrs after incubation, the cells were washed and loaded with MitoTracker reagents.

Lactate quantification.

Lactate was quantified according to the manufacturer's protocols (Sigma-Aldrich). Colonocytes were resuspended in 4 volumes of lactate assay buffer, sonicated 10 cycles and centrifuged (13,000g, 10min). Samples were deproteinized with a 10-kD molecular weight cut-off spin filter. A master reaction mix containing 46µl lactate assay buffer, 2µl lactate enzyme mix, and 2µl lactate probe was added on 50µl sample solution. Reactions were incubated at RT for 30 min and absorbance measured at 570 nm on a microplate reader.

Fecal extracts preparation.

100mg of mice feces were homogenized in 1ml of Phosphate buffer saline containing 50µg/ml gentamycin, 100Units/ml penicillin and 100µg/ml streptomycin. The homogenate was

centrifuged (10000rpm, 15min, 4°C) and the supernatant filtrated on a Nanosep column with 3K Omega (Pall). The eluate was immediately used to treat the cells.

Organoid culture and stimulation.

For experiments with 2D organoids in Air-Liquid Interface (ALI), we followed the previously described protocol (Wang, Chiang et al. 2019). Briefly, cultured mouse colon organoids were dissociated in single cells and seeded on polycarbonate transwells, with 0.4µM pores (CORNING). Initially, cells were seeded in the presence of 50% L-WRN media with 10µM Rock inhibitor Y-27632 in both the lower and the upper chamber. After 7 days, the media was removed from the upper chamber to create an ALI. Cells were maintained in these conditions for 14 days to establish a homeostatic monolayer.

2D organoid cultures were exposed to 30ng/ml TNFa for 3 days and epithelial restitution was assessed 2 days after TNFa withdrawal. During the experiments, colon organoids were treated or not with 500µM pantethine (Sigma-Aldrich), or 1µM rosiglitazone (Sigma-Aldrich), or 1µM BADGE (Sigma-Aldrich). Cell death was evaluated by immunofluorescence using the zombie red stain (Biolegend). Quantification of the percentage of zombie red positive cells was performed on microscope confocal images (Carl Zeiss LSM 880) using the ImageJ software (NCBI). For epithelial recovery, qRT-PCR were performed to explore the expression of Muc2 and Ang4.
